

Seismic Response Analysis of a Multi-Span Curved Continuous Box-Girder Bridge with Multiple Supports

By

Yifan Wang

April 2022



Department of Civil Engineering and

Applied Mechanics

McGill University, Montreal

Thesis submitted to the Faculty of Graduate Studies and Research in partial fulfillment of
the requirements of the degree of Master of Engineering

© 2022 Yifan Wang

Abstract

Curved concrete box-girder bridges are widely applied in highway systems to enable traffic to move from one highway to another. The Akşemsettin Viaduct (termed A Viaduct in the current study) in Istanbul, Turkey, is a typical 11-span curved continuous bridge with a total length of 596.8 m. Located in the high seismicity zone, the A Viaduct exhibits complex seismic behaviour because varying ground motion inputs are expected to excite the bridge at different column/abutment foundations. This study investigates the seismic responses of the A Viaduct under different ground motion scenarios using nonlinear time history analyses (NTHAs). In particular, the software of OpenSees is used to develop a high-fidelity finite element model for the A Viaduct, from which seismic responses of multiple critical components are compared under uniform versus multiple support excitations. To supplement such comparisons, a literature survey is conducted regarding seismic damage to curved bridges, their soil-structure interaction effect, and the multi-support excitation scheme. Moreover, modelling considerations of key components are presented for the A Viaduct, and 6 representative groups of simulated ground motions are selected to capture the effects of site-specific surface topography and soil stratigraphy at the bridge site.

Résumé

Les ponts caissons-poutres en béton incurvés sont largement appliqués dans les systèmes autoroutiers pour permettre au trafic de passer d'une autoroute à une autre. Le viaduc Akşemsettin (appelé viaduc A dans la présente étude) à Istanbul, en Turquie, est un pont continu courbe typique à 11 travées d'une longueur totale de 596,8 m. Situé dans une zone de forte sismicité, le viaduc A présente un comportement sismique complexe car des mouvements du sol variables sont susceptibles d'exciter le pont au niveau des différentes fondations des colonnes et des piliers. Cette étude examine les réponses sismiques du Viaduc A sous différents scénarios de mouvement du sol en utilisant des analyses non linéaires de l'histoire du temps (NTHA). En particulier, le logiciel OpenSees est utilisé pour développer un modèle d'éléments finis haute-fidélité pour le Viaduc A, à partir duquel les réponses sismiques de plusieurs composants critiques sont comparées sous des excitations uniformes et des excitations à supports multiples. Pour compléter ces comparaisons, une étude documentaire est menée sur les dommages sismiques causés aux ponts courbes, sur les effets de l'interaction sol-structure et sur le schéma d'excitation multi-supports. De plus, les considérations de modélisation des composants clés sont présentées pour le Viaduc A, et 12 groupes représentatifs de mouvements de sol simulés sont sélectionnés pour capturer les effets de la topographie de surface et de la stratigraphie du sol spécifiques au site du pont.

Acknowledgements

The author entered McGill University in 2020, and it is now the second year. From a new student who was ignorant at the beginning to a prospective graduate who will continue his work overseas, I have grown up a lot under the guidance of my teachers and company friends during this period. During the two years of study, the teachers' teachings and peers' help have made me realize the way of research and life.

First of all, I would like to thank my thesis supervisor, Prof. Yazhou Xie, who provided me with a good environment and showed me the direction of my research during my study. I was impressed by her profound knowledge of earthquake research, which laid the foundation for me to continue my engineering-related work in the future. In my daily life, my teacher is easy-going and often cares about my future development and life situation, which also creates a good living atmosphere for me. I wish you all the best in your future endeavours.

This work is a part of a collaborative project that involves several researchers in Turkey, United States, and other countries. Thank Dr. Asli Kurtulus and Prof. Ertugrul Taciroglu from UCLA for initiating and managing this multi-institutional project. Design plans of the bridge are provided by Turkish General Directorate for Highways; input ground motions are developed by Dr. Wenyang Zhang through the support from The Scientific and Technological Research Council of Turkey (TUBITAK Grant No.116M232). Their efforts and the funding support are greatly appreciated.

I would also like to thank all my instructors, Prof. Luc. E. Chouinard, Prof. Ghyslaine McClure, Prof. Mohamed Meguid, and Prof. Denis Mitchell, in my two years of graduate studies for their guidance, and I would like to express my heartfelt thanks to them.

I would like to thank my peers for their support during my two years of study. I would also like to thank my groupmates, Chunxiao Ning, Han Lin, Simon Law, Sirui Song, Yihan Shao, Xuejiao Long, and Zinan Zhang, for their help in life and study.

I also thank the examiners who reviewed my work in their busy schedules.

Wang Yifan

April 2022, Montreal, Snow

Table of Content

Abstract.....	1
Résumé.....	2
Acknowledgements.....	3
1. Introduction.....	6
1.1. Seismic damage to multi-span curved viaducts	6
1.2. Soil-structure interaction	7
1.3. Multi-support analysis of ground motions	9
1.4. Research objective.....	11
1.5. Thesis outline	11
2. Bridge Design of the Akşemsettin Viaduct in Istanbul.....	13
2.1. Geometry and overall design consideration	13
2.2. Geological condition at the bridge site.....	15
2.3. Deck.....	15
2.4. Column	16
2.5. Bearing	17
2.6. Abutment.....	18
2.7. Foundation.....	19
3. Numerical Modelling of the A Viaduct in OpenSees.....	20
3.1 Overall modelling considerations	20
3.2. Deck.....	22
3.3. Column	22
3.4. Bearing	23
3.5. Abutment components.....	25
3.6. Foundation.....	28
4 Physics-based Simulations of Ground Motions at the A Viaduct	32
4.1. Overall methodology	32
4.2. Selected ground motions	32
5. Seismic Response Analyses of the A Viaduct Under Different Motion Inputs.....	36

5.1. Uniform excitation	36
5.2. Multi-support excitation	36
5.3. Response comparisons of critical bridge components	36
6. Conclusion	44
Reference	46
Appendix A – All Sets of Ground Motion Records	53
Appendix B - Responses of Bridge Columns and Bearings	61

1. Introduction

1.1. Seismic damage to multi-span curved viaducts

Horizontally curved viaducts are widely utilized in transportation networks for interchanging roadways. Curved viaducts have been extensively constructed in the last 30 years; these bridges account for about one-third of all bridges under construction today in the United States [1]. Stress, strain, and internal forces have complex distributions in curved viaducts, particularly for those with slight curvatures [2]. Due to the existence of the horizontal curvature, viaducts undertake not only bending moments and shear forces, but also substantial torsional moments (e.g., the bending-torsion coupling effect). These moments would rotate the axes of principal stresses, thereby increasing the risk of concrete cracking and other damage mechanisms.

In addition, the seismic response of irregular curved viaducts supported on columns with unequal heights, particularly for those crossing valleys, turns out to be a challenging problem that requires extra attention. Due to geometric irregularities, the center of mass offsets the center of rigidity, increasing the possibility of in-plane rotating of the deck [3]. If such rotations are significant, the transverse displacement at the end of the deck might be increased, which may cause the bridge to be unseated. The increased eccentric displacement may also cause bridge piers to deform in shear and torsion. Researchers started to investigate the seismic resistance of curved viaducts after the significant damage to the SR14/15 interchange of Golden State highway during the 1971 San Fernando Earthquake (Fig 1.1). Despite several research efforts since 1971, curved viaducts still exhibited severe damage after recent earthquake events; these damages included span unseating and complete collapse. For example, the Huilan interchange had a bending-shear failure at the short pier near the abutment, and the Baihua viaduct collapsed (Fig 1.2) during the 2008 Wenchuan Earthquake in China.



Fig 1.1 Failure of the SR14/15 Interchange



Fig 1.2 Failure of the Baihua bridge

1.2. Soil-structure interaction

The multi-span curved viaduct also requires specific consideration of the soil-structure interaction (SSI) effect. The SSI effect would significantly alter the seismic performance of the bridge-soil system in several aspects. First, SSI changes the wave-field of the input seismic force compared with free-field motions. Due to the flexibility of the supporting soil, the stiffness of the bridge-soil system is lower than the bridge itself. Meanwhile, the existence of soil radiation damping would also increase structural damping [8-11]. By contrast, bridges would change both soil's static force field and the dynamic transmission path of seismic waves in soils. In dealing with these different aspects of SSI, previous studies can be divided into the following three phases:

- (1) From the 1950s to the 1960s, studies focused on deriving the transient and stationary theoretical solutions of vibrations of circular and rectangular plates surrounded by semi-infinite soil domains [16-18].
- (2) From the 1970s to the 1980s, numerical simulations became a major pathway to solving SSI problems, benefitting from the development of finite element methods, finite difference methods, and boundary element methods [19-20].
- (3) After the 1990s, scholars investigated the SSI effect by carrying out a large number of field and experimental tests and combining them with theoretical analyses or numerical simulations [23-25].

Since SSI deals with material nonlinearity and nonlinear interaction, the traditional analytical methods developed in the early 1960s can only solve individual problems under specific simplified conditions. From the practice perspective, existing approaches to analyze SSI effects in bridges include substructure, direct, and lumped parameter methods.

The basic idea of the substructure method is shown in Fig 1.10, which separates the soil-structure system into structure system (substructure 1) and foundation-soil system (substructure 2). The method analyzes the soil substructure according to external loads and also determines the structural loads from the soil. Finally, the dynamic response of the structure is solved using structural loads from the soil with proper interface constraints. The substructure method reduces the degrees of freedom of the structure and improves computational efficiency. However, the method essentially applies the superposition principle, which remains difficult to deal with any nonlinearity and is hard to simulate the energy exchange between soil and structure. As a result, computational accuracy remains questionable when using the substructure method.

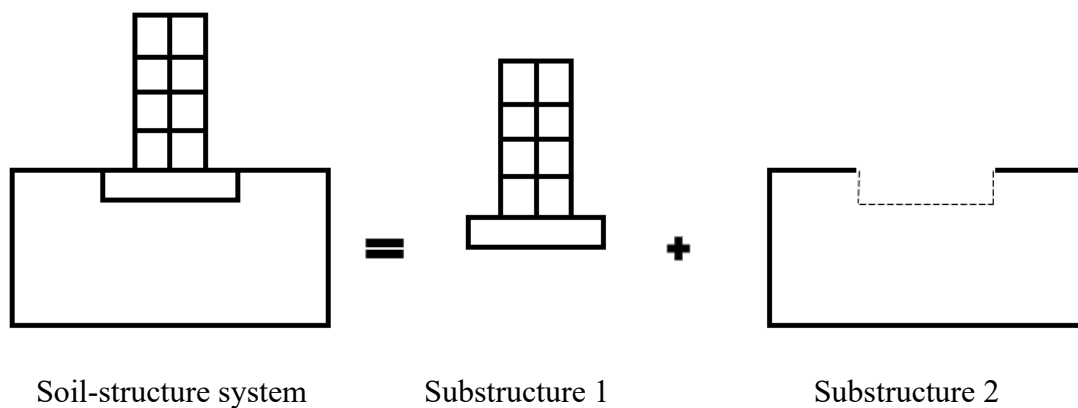


Fig 1.10 Schematic plot of the substructure method

The direct method regards bridge, foundation, and soil as an integrated system and analyzes the dynamic response of the entire system, during which the SSI effect is captured automatically. The direct method commonly relies on numerical simulation approaches such as the finite element method, finite difference method, boundary element method, etc. [27-29]. In particular, the finite element method is able to deal with challenging problems that include

significant nonlinearity and cover multiple fields at large scales. Nevertheless, this approach is computationally expensive and complicated, limiting its real-world implementations.

The lumped parameter method simplifies the semi-infinite soil-foundation into spring-damping-mass systems and uses lumped parameters to represent the dynamic resistances of foundation and soil [17]. This approach is promising in engineering applications. For example, spring-mass models are utilized in the Japanese Immersed Tunnels Seismic Code to simulate the soil when computing the vertical seismic responses of tunnels [30]. Conversely, the lumped parameters method also has its shortcomings. For instance, linear springs have been used most of the time by neglecting soil nonlinearity; the seismic wave on the free surface is also commonly considered the earthquake input without taking into account any wave-field interaction from the structure. In this study, the lumped parameter method is used to simulate the SSI effect of the A Viaduct, where nonlinear springs are used to capture foundation-soil behaviours at both column and abutment foundations. In particular, the multi-support analysis scheme is considered for ground motion excitations.

1.3. Multi-support analysis of ground motions

Local topography may induce variances in frequencies and amplitudes of seismic waves when the construction field of the bridge has a varying topography. This phenomenon is known as the spatial variation of seismic ground motions at different supporting points of the bridge. Sometimes, such topographic effects can generate magnified seismic waves [31-32]. The bridge foundations may also receive seismic excitations at different time instants when the transmission direction of the seismic wave is similar to the layout direction of bridge piers. According to field tests, seismic excitations received by supporting points of large-span structures may have significant time differences within 50 meters [33]. In recognizing such topographic effects, it is required to account for the local site effect when analyzing long bridges under seismic loading [34]. The local site effect becomes more prominent and complex when dealing with multi-span curved bridges (e.g., the A Viaduct) that show significant spatial irregularity, in which case multi-support excitations need to be considered.

Previously, several studies handled multi-support excitations when analyzing bridges under earthquake loads. The bridge's dynamic response pattern under the travelling wave effect

was investigated by Bogdanoff (1965) [35], who confirmed the need to utilize multi-support excitations to capture earthquake ground motions' spatial variation. K. Soyuluk (2004) [36] investigated the effect of seismic multi-support excitations on long-span bridges using the random vibration method. The feasibility of using a filtered white noise ground motion model to represent the natural ground motion is validated. Similarly, Liang et al. (2006) [37] developed the average response spectrum method to analyze the dynamic response of bridges under spatially varying earthquake ground motions. Their results revealed that the ground motion spatial effect might magnify the structures' inertial forces. By considering multi-support excitation, Liang et al. (2007) [38] also investigated the seismic capacity of steel truss arch bridges. Amplified seismic response of the truss arch bridge has been observed due to multi-support excitations.

Recently, Burdette et al. (2008) [39] discussed the effect of non-uniform excitations on the seismic responses of curved girder bridges from the perspective of geometric incoherence in travelling seismic waves. They conducted NTHAs using a finite element bridge model with 8 spans and a radius of 200 m. The result showed that the bridge response is amplified significantly when subjected to asynchronous seismic ground motions. Alexander (2008) [40] carried out a multi-support excitation analysis to investigate the dynamic response pattern of a single span bridge when subjected to recorded ground motions. This study indicated that uniform support excitation analysis might be too conservative for spatially heterogeneous ground motion inputs. Jia (2013) [41] examined the nonstationary stochastic vibration of a high-pier railway bridge under tridirectional spatially varying excitations and derived a nonstationary stochastic analysis scheme.

In summary, existing methods to incorporate multi-support excitations in bridges include deterministic NTHAs, random pseudo excitation method, and multi-support excitation response spectrum method. Deterministic NTHAs rely on individual groups of time history excitations to represent seismic loads. The multi-support excitation is realized by inputting seismic waves with different durations, amplification, and frequency spectra at different pier foundations. The random pseudo excitation method assumes that ground motion is a random process in time and space. Therefore, spatial correlation functions are used to describe the

correlation of ground motions at different locations. This method computes the statistical properties of bridge responses using the auto-power spectrum or cross-power spectrum of the seismic ground motion field. The multi-support excitation response spectrum method is similar to the traditional response spectrum method. However, it also takes into account the extra spatial-temporal characteristics of ground motions when developing the seismic response spectrum of civil engineering structures. This method appears in different design codes when multi-support excitation is of concern. Deterministic NTHAs are considered in this study to analyze the A Viaduct with multiple supports.

1.4. Research objective

The main objective of this thesis is to determine the seismic response of a multi-span curved continuous bridge under different types of excitations through a numerical study using OpenSees. In particular, this research attempts to:

- (1) Develop finite element models to carry out time-history analysis of the multi-span curved continuous bridge.
- (2) Evaluate the seismic response, including the displacement and force of critical components of the A Viaduct.
- (3) Explore to what extent different ground motion excitation schemes would change the seismic response of the bridge.

1.5. Thesis outline

The thesis is organized into six subsequent chapters with the following contents (Figure 1.11):

Chapter 2 presents an overall discussion about the geological condition of the A Viaduct. This chapter also presents the physical properties of critical components, such as the superstructure, columns, abutments, foundations, bearings, and impact elements.

Chapter 3 provides modelling details for various bridge components. The chapter also presents the integration of various component models to generate the global numerical model of the bridge for NTHAs.

Chapter 4 illustrates the ground motions used to derive the multiple support excitation scheme.

Chapter 5 quantifies the seismic responses of different bridge components under three

ground motion excitation scenarios.

Finally, a summary and discussion of future work are presented in Chapter 6.

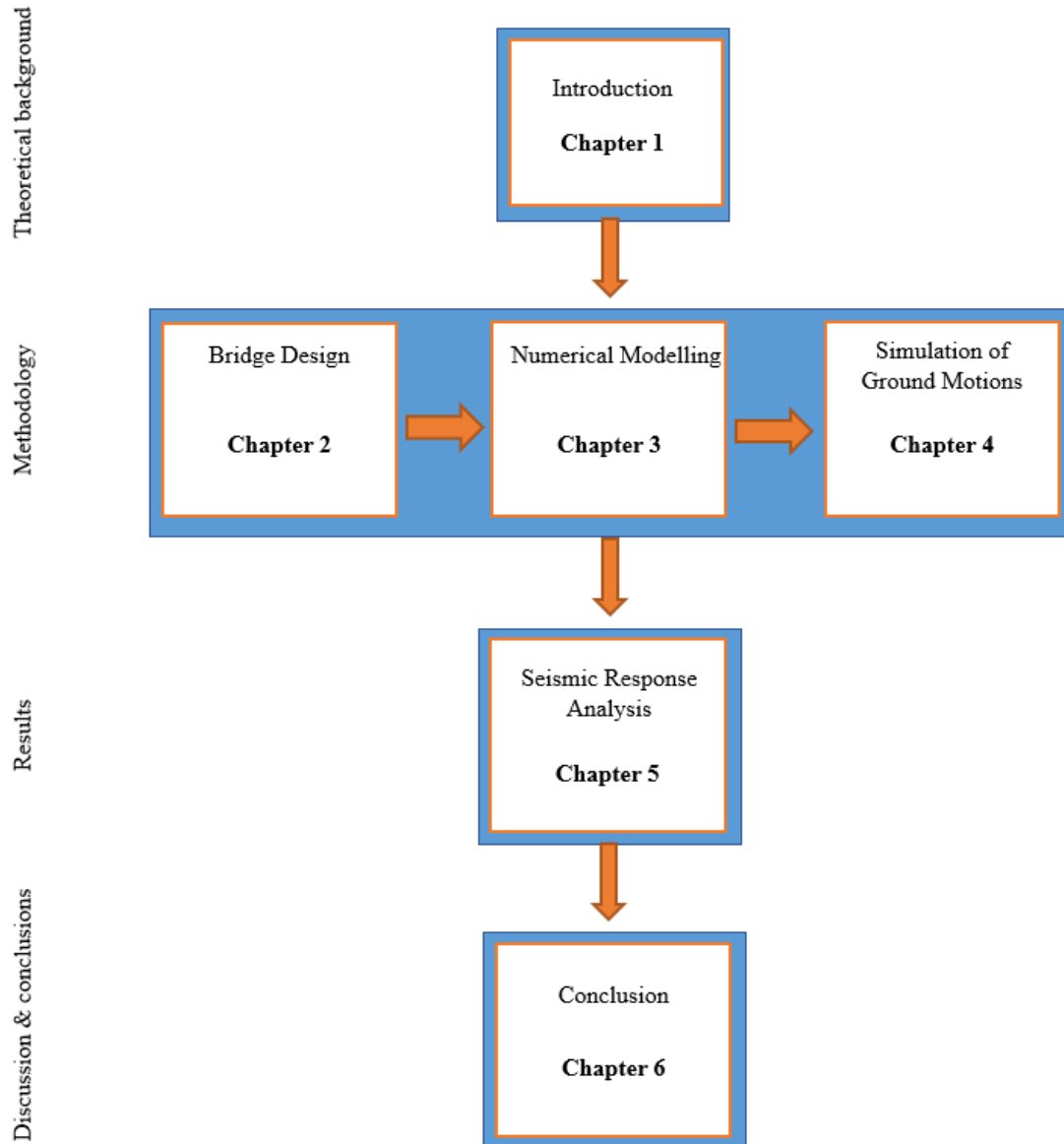


Fig 1.11 Flowchart of the dissertation layout

2. Bridge Design of the Akşemsettin Viaduct in Istanbul

2.1. Geometry and overall design consideration

As shown in Figure 2.1, the A Viaduct considered in this study locates in the city of Istanbul, Turkey (41.094°, 28.921°). Due to site-specific topographic conditions, the viaduct was constructed in the form of a horizontally curved concrete bridge with a planar curvature of 1500 m and a slight gradient in the vertical direction. The bridge has a total of 11 spans with 10 column piers and two end abutments. The first and last spans have a length of 46.4 m; the length for the sixth span is 40 m; other spans are 58 m in length. Therefore, the total length of the bridge is 596.8 m. The deck placed over the abutment has a width of 20 m. Besides, the heights of the bridge deck at the highest point from the ground varied from 17.64 m to 35.28 m. Bridge piers are designed with rectangular hollow sections with dimensions of 3.0 m × 7.0 m and a thickness of 0.45 m. The height of column sets P1-P7 is around 25 m, and the pier sets P8-P10 are less than 20 m in height. The bridge deck and piers/abutments are connected through bearings. The piers at P1 and P7-P10 are supported by shallow foundations, and the piers at P2-P6 are supported by pile foundations, each consisting of 16 piles with a diameter of 1.65 m and lengths varied from 13.5 m to 41.5 m. The piles were constructed with C25 in concrete and S200 in steel reinforcement.

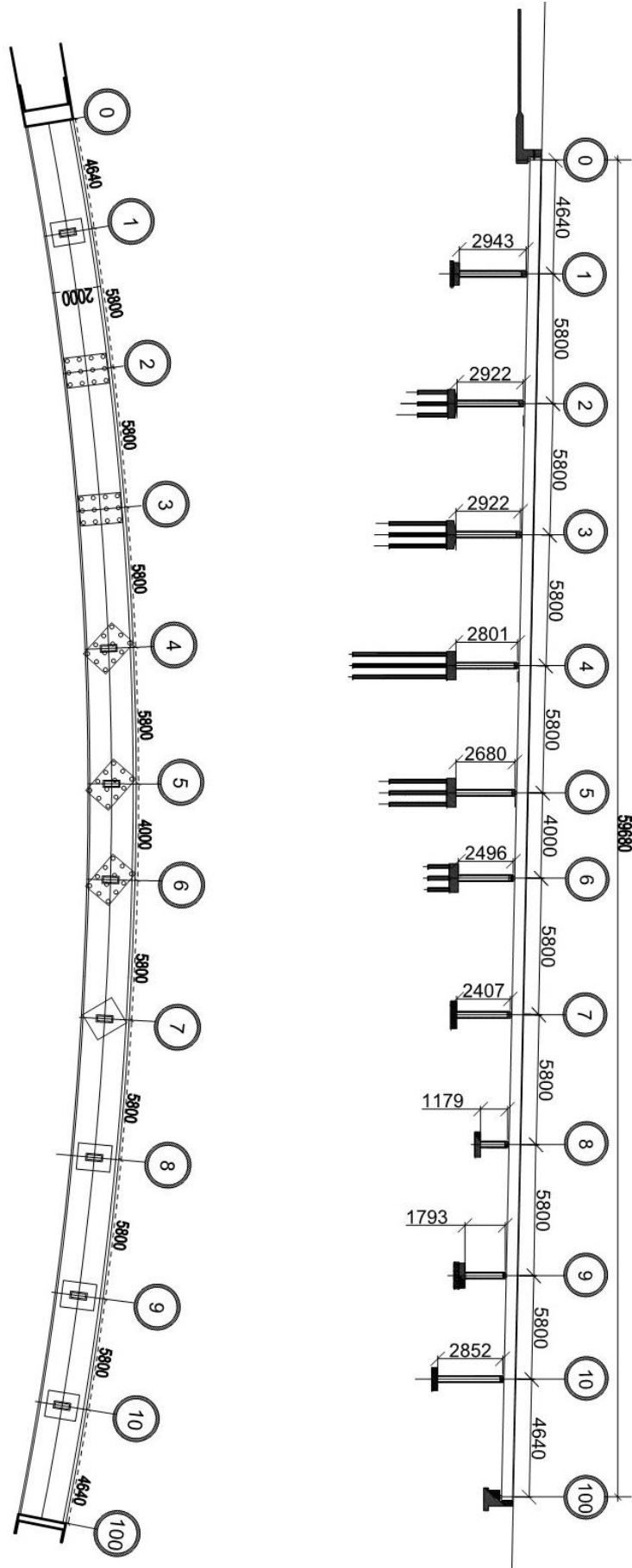


Fig 2.1 Design Information of the A Viaduct

2.2. Geological condition at the bridge site

Four drillings at depths varying between 12 m - 40 m were carried out at the bridge site. The Standard Penetration Test (SPT) was performed on the soils. As listed in Table 2.1, soil classes have been determined for each soil layer, together with the associated soil properties, including soil type (cohesive - C or non-cohesive - S), soil layer thickness H , unit volume weight γ_n , effective stress at the middle of the layer σ'_m , effective stress at the end of the layer σ'_e , standard penetration resistance N , and shear wave velocity V_s . In general, the soils at the bridge site can be divided into 4 layers, namely the manmade sandy fill with $V_s = 180$ m/s, the pebbled sand layer with $V_s = 227.51$ m/s, the silty clay layer with $V_s = 200$ m/s, and the bottom sandstone layer with $V_s = 693$ m/s.

Table 2.1 Engineering Parameters and Properties of Sub-Foundation Soils of the A Viaduct

Soil Type	C/S	H (m)	γ_n (kN/m ³)	σ'_m (kPa)	σ'_e (kPa)	N	V_s (m/s)
Manmade Fill	C	5.5	17	46.8	78.5	-	180.00
Pebbled Sand	S	4.5	19	98.8	119	30	227.51
Silty Clay	C	25	19	231.5	344	8	200.00
Sandstone	C	5	23	401.5	459	-	693.00

2.3. Deck

As presented in Figure 2.2, the A Viaduct uses the single-cell cast-in-place concrete box-girder as the bridge deck. The concrete material is C35. The box-girder has a height of 5.05 m, a top-slab width of 19.3 m, and a bottom width of 7 m. In particular, the thickness of the box-girder varies linearly from the middle span to the bridge ends, where a solid cross-section is designed for the bridge deck.

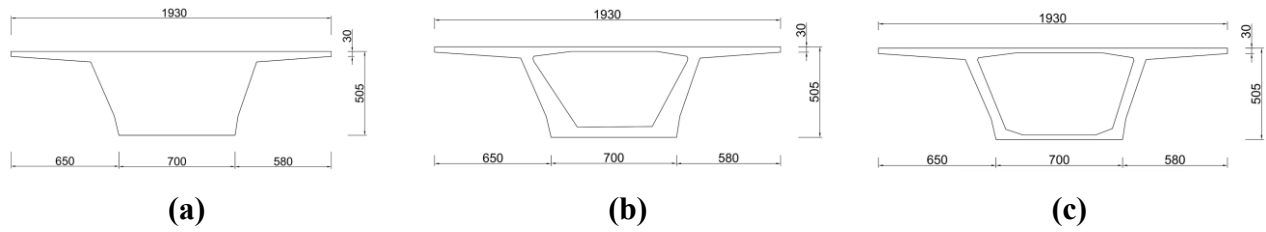


Fig 2.2 Dimensions of Girder Cross Sections at (a) Bridge ends, (b) Column ends, and (c) Middle Spans (unit: cm)

2.4. Column

Bridge interior bents, denoted as P1-P10 in Figure 2.1, are designed with rectangular C25 concrete columns with an external dimension of 3.0 m \times 7.0 m. The columns have a hollow box cross-section with a thickness of 0.45 m (Figure 2.3). As shown in Figure 2.1, the column heights vary from 11.79 m to 27.43 m. Figure 2.3 also indicates that longitudinal reinforcements are placed in both exterior and interior rows of the column. With a diameter of 12.5 mm and a total rebar number between 244 and 296, the reinforcement ratio of the column varies from 1.46% to 1.83%. Transverse reinforcements in the column are designed with #4 confinement rebars with a spacing of 150 mm. The clear concrete cover for confinement rebars is 40 mm. In addition to the hollow section shown in Figure 2.5, a solid cross-section with a height of 2.0 m and a material type of C35 is designed at the column top to place bearings and connect to the deck.

Table 2.1 Longitudinal Reinforcement Information in the Columns

Column Number	Number of Reinforcements	Diameter of Bars (mm)	Reinforcement Ratio
P1	244	12.5	1.46%
P2	260	12.5	1.56%
P3	292	12.5	1.83%
P4	252	12.5	1.51%
P5	296	12.5	1.77%
P6	244	12.5	1.46%
P7	252	12.5	1.51%
P8	244	12.5	1.46%
P9	244	12.5	1.46%
P10	244	12.5	1.46%

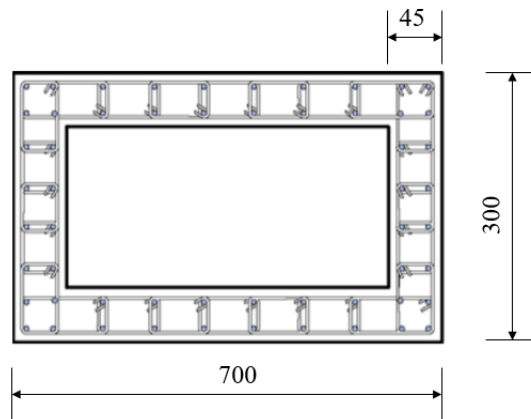


Fig 2.3 Dimensions and Steel Arrangements of the Column (unit: cm)

2.5. Bearing

The A Viaduct is designed with a combination of elastomeric and sliding bearings to isolate the bridge deck. As shown in Figure 2.4, ten elastomeric bearings are placed at the top of the columns to constrain the transverse placements of the bridge deck. In the longitudinal direction, P1 to P4 columns are designed with elastomeric bearings, while the remaining columns are installed with sliding bearings. Tow bars are used at the left abutment, while a sliding bearing is also placed at the top of the right abutment. The general dimensions and placements of all bearings are listed in Table 2.2.

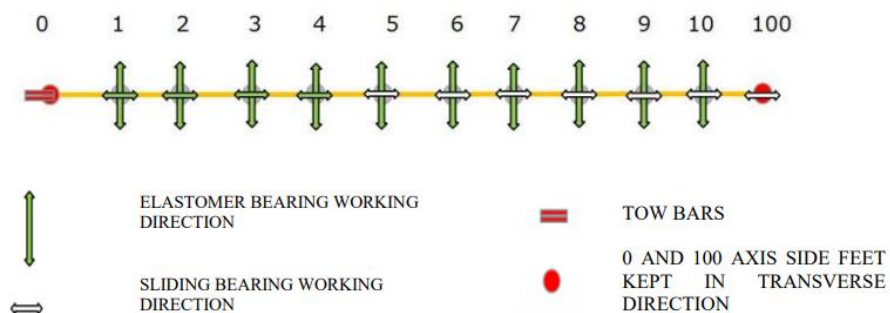


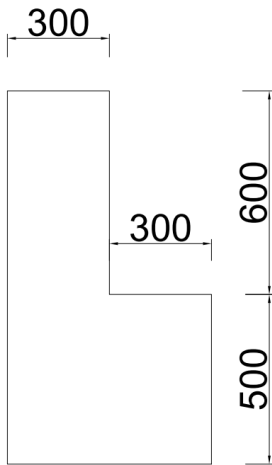
Fig 2.4 Arrangement of Both Elastomeric and Sliding Bearings

Table 2.2 Dimensions and Placements of Bearings

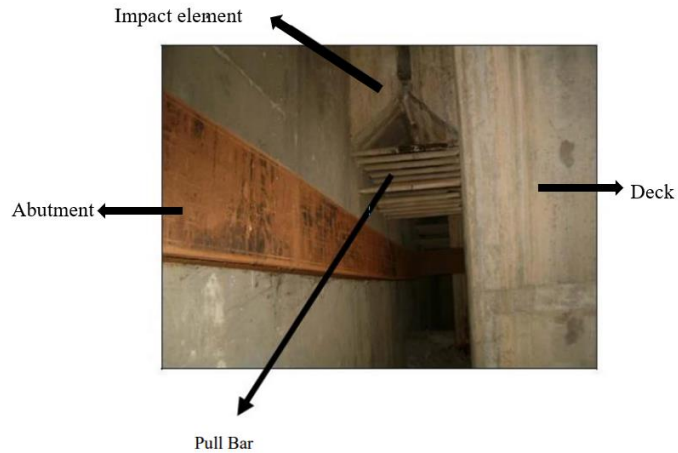
Location	Dimension (mm)			Number	Direction	Sliding Direction
	Length	Width	Height			
P0	800	800	109	2	X	-
P1	800	800	109	4	X-Y	-
P2	800	800	109	4	X-Y	-
P3	800	800	129	4	X-Y	-
P4	800	800	209	4	X-Y	-
P5	700	800	109	4	Y	X
P6	700	800	129	4	Y	X
P7	800	800	189	4	Y	X
P8	800	800	109	4	Y	X
P9	800	800	109	4	Y	X
P10	800	800	109	4	Y	X
P100	800	800	109	2	-	X

2.6. Abutment

Solid concrete blocks are designed for the abutment stem wall and the back wall; their dimensions are presented in Figure 2.5 (a). Additional pull bars are also designed to connect the bridge deck to the back wall, preventing the bridge from moving in the longitudinal direction. As shown in Figure 2.5 (b), a total of 58 steel pull bars are designed at the west abutment to provide the tensile constraint, whereas the compressive constraints at both abutments are achieved through the shear key-type impact element between the deck and the back wall.



(a) Dimensions of the Abutment Walls



(b) Impact Element and Steel Pull Bars at the West Abutment

Fig 2.5 Elements at End Abutment

2.7. Foundation

Bridge bent P2, P3, P4, P5, and P6 are designed with pile foundations. Each pile foundation consists of 12 bored piles arranged in 3 rows and 4 columns (Figure 2.6); the piles all have a diameter of 1.65 m and a varied length between 9.5 m and 41.5 m, as illustrated in Figure 2.1. The pile foundations are designed with pile caps in-plane dimensions of 12.5 m × 17.5 m and thickness of 3 m or 4 m. Other than pile foundations, bridge bent P1, P7, P8, P9, P10, and end abutments P0 and P100, are designed with spread footings (Figure 2.1). These shallow foundations have a plane dimension that varies from 10.0 m × 13.0 m to 12.2 m × 14.0 m, 11.0 m × 14.0 m, and 11.0 m × 13.0 m. All spread footings are designed with a height of 2.5 m.

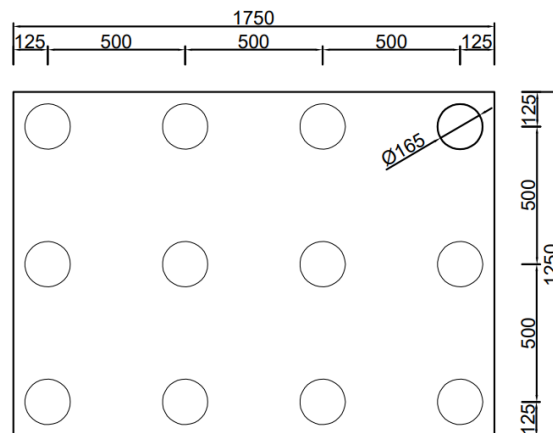


Fig 2.6 Pile Arrangement of the Pile Foundation

3. Numerical Modelling of the A Viaduct in OpenSees

3.1 Overall modelling considerations

The software platform of OpenSees [51] is used to develop the numerical model for the A Viaduct. As shown in Figure 3.1, the deck in one span is treated as a spine with multiple elastic beam-column elements along the centerline of the bridge. Tributary masses are lumped at two end nodes for each element. Rigid and massless beam elements are used to model the transverse diaphragms at bridge bents and end abutments; these rigid elements are also used to place bearings for being connected to the columns and other abutment components. The weight density of reinforced concrete is assumed to be 25 kN/m^3 ; 23650 MPa is used as Young's modulus of concrete, and the Poisson ratio is 0.2. The P-Delta effect is also triggered during the NTHAs. Two horizontal ground motions are applied as excitations at each column and abutment foundation. As such, the free nodes of the foundation elements are constrained in the vertical translational direction and three rotational directions. Overall modelling considerations for each bridge component are also illustrated in Figure 3.1; they will be discussed in detail in the following sections.

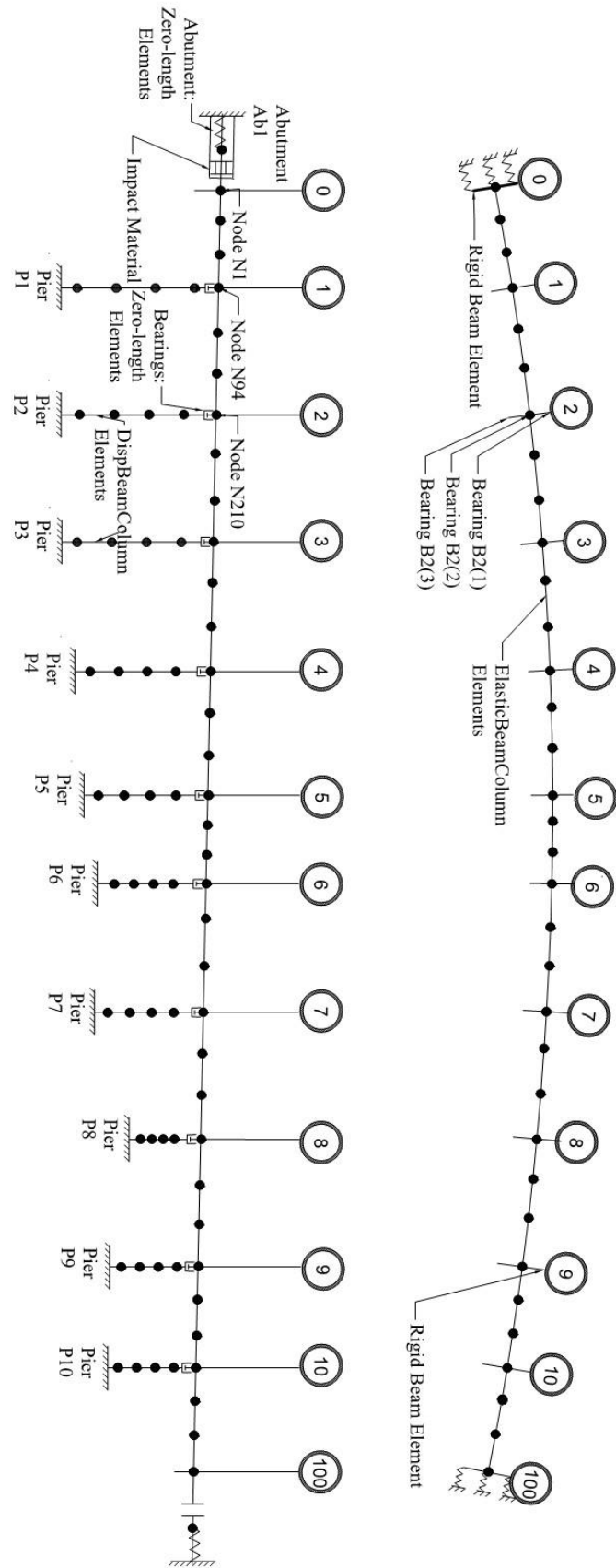


Fig 3.1 Overall Modelling Considerations for the A Viaduct

3.2. Deck

As mentioned, elastic beam-column elements are adopted to simulate the bridge deck. The element size is chosen as 0.5 m to emulate the curved shape of the deck. The geometric, mass, and inertia properties of the deck cross-sections are calculated based on the design drawings of the deck; these values are tabulated in Table 3.1. Three different sections are considered to model the bridge deck – a solid section with a total length of 4 m at bridge ends; a thick hollow section with a total length of 5 m at each side of column support; and a regular thin hollow section at the middle of each span. Due to different reinforcement arrangements, the unit weight of the bridge deck at the middle span is larger than that at end spans and near column supports.

Table 3.1 Geometric and Mass Properties of the Bridge Deck

Property	Location	Value
Area	Middle Span	15.20 m ²
	Near Column	20.00 m ²
	End Span	47.45 m ²
Unit Weight	Near Column & End Span	27.34 kN/m ³
	Middle Span	28.08 kN/m ³
Translational Mass	Middle Span	21.77 t/element
	Near Column	27.88 t/element
	End Span	66.19 t/element

3.3. Column

As shown in Figure 3.2, columns are modelled using twelve fiber-type displacement-based beam-column elements along with rigid links at the column top and bottom, simulating the solid sections at these two locations. In the fiber sections, the unconfined and confined concrete are simulated using the *Concrete02* material; the constitutive relationship of the confined concrete is simulated using the Kent-Park model [52]. The *Steel02* material with the Giuffr -Menegotto-Pinto model for isotropic strain hardening [53] is utilized to model the longitudinal reinforcements in the column. The torsional stiffness of the column is computed using the moment of torsion times shear modulus. The translational and rotational masses are lumped at

the nodes of the column elements.

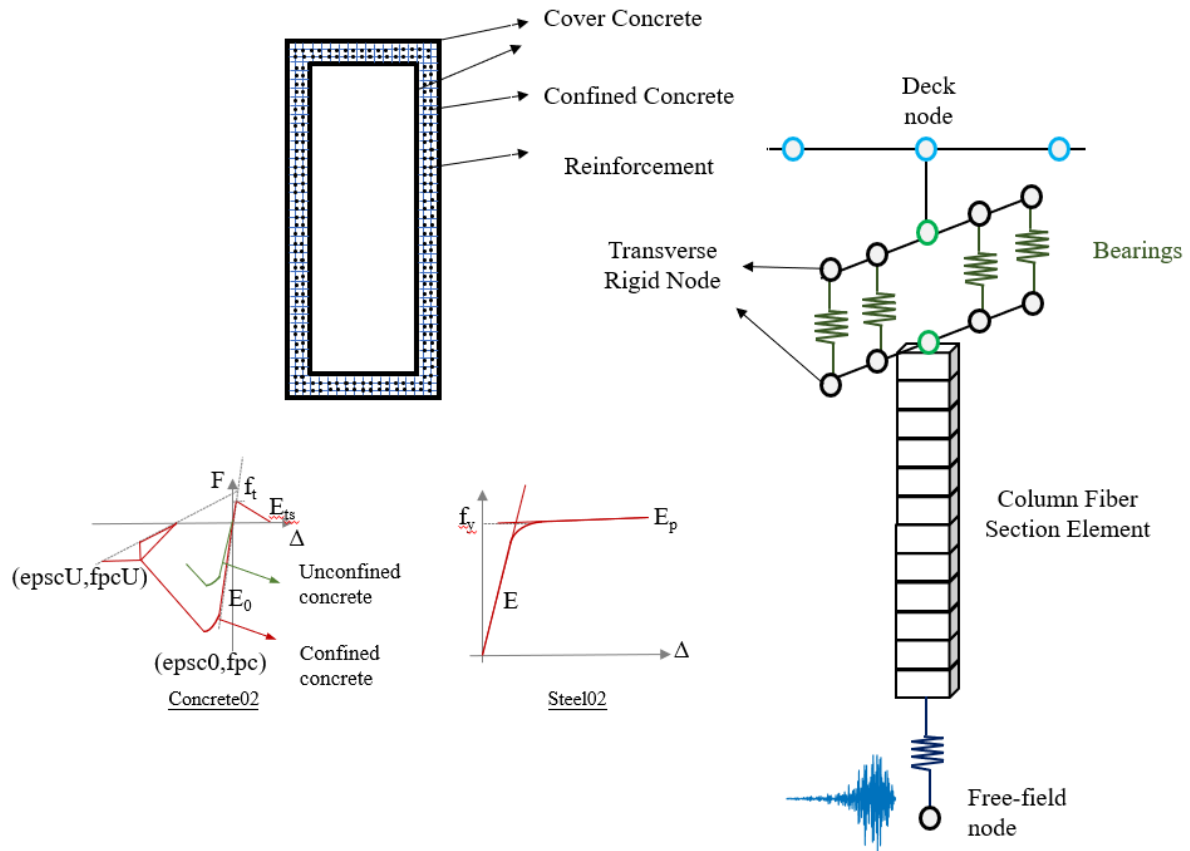


Fig 3.2 Overall Modelling Considerations for Bridge Bents

3.4. Bearing

Previous studies [54] proved that the shear force-displacement hysteric loop of elastomer and sliding bearings could be approximated using a bilinear model, as shown in Fig 3.3. In particular, the bearing's horizontal restoring force can be computed as:

$$F(x) = \begin{cases} K_1 \cdot x, & x < x_y \\ K_2 \cdot x, & x \geq x_y \end{cases} \quad (3.1)$$

where x is the relative displacement above and below the bearing, K_1 is the elastic stiffness, K_2 is the post-yielding stiffness, and x_y is the yielding displacement, which is assumed as the value equal to h_{eff} in the current study, where h_{eff} is the effective bearing height.

Shear modulus G of the elastomeric bearing material is between 0.9 - 1.38 MPa, where the

mean value of 1.14 MPa is utilized in the current work. Therefore, the elastic stiffness of elastomer bearings is computed using the following equation.

$$K_1 = \frac{AG}{h_{eff}} \quad (3.2)$$

where A is the area of elastomer bearings. Besides, the post-yielding stiffness of the elastomeric bearing is determined by defining the stiffness ratio N ($N = K_1 / K_2$). A common ratio of $N = 10$ is considered for the elastomer bearings.

Previous research also revealed that the hysteric loop of sliding bearings is similar to the elastic-perfectly plastic material, as shown in Figure 3.3. Therefore, for sliding bearings, the stiffness ratio N can be taken as a large value, such as 50 [54], and its horizontal restoring force can be computed as:

$$F_{max} = K_1 \cdot x_y = \mu_d \cdot R \quad (3.3)$$

where F_{max} is the critical friction force, μ_d is the sliding bearing friction factor and taken as 0.04, and R is the support reaction provided by the bearing and x_y is the yielding displacement, which is assumed as 0.2 m in the current study. The modelling parameters of both elastomeric and sliding bearings are summarized in Table 3.2.

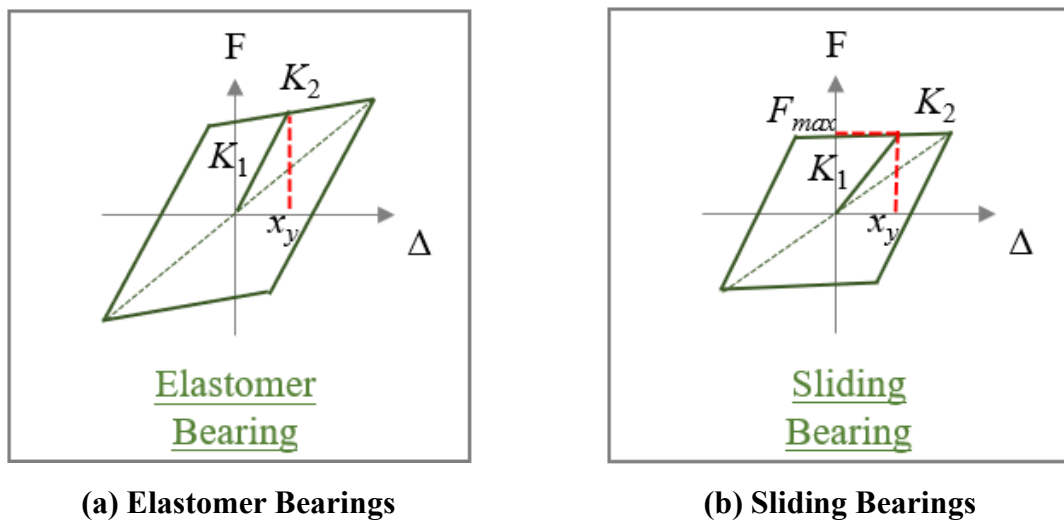


Fig 3.3 Bilinear Models for Modelling Bearings

Tale 3.2 Modelling Parameters of both Elastomeric and Sliding Bearings

Location	Area (m ²)	H _{eff} (mm)	Longitudinal Direction			Transverse Direction		
			Bearing Type	K ₁ (kN/m)	N	Bearing Type	K ₁ (kN/m)	N
Abutment	0.64	85	EBs ¹	8584	10	EBs	8584	50
P1	0.64	85	EBs	8584	10	EBs	8584	50
P2	0.64	85	EBs	8584	10	EBs	8584	50
P3	0.64	101	EBs	7224	10	EBs	7224	50
P4	0.64	165	EBs	4422	10	EBs	4422	50
P5	0.56	85	SBs ²	1300	50	EBs	7511	50
P6	0.56	101	SBs	1300	50	EBs	6321	50
P7	0.64	149	SBs	1300	50	EBs	4897	50
P8	0.64	85	SBs	1300	50	EBs	8584	50
P9	0.64	85	SBs	1300	50	EBs	8584	50
P10	0.64	85	SBs	1300	50	EBs	8584	50
Abutment	0.64	85	SBs	1300	50	EBs	8584	50

¹ Elastomeric Bearings; ² Sliding Bearings.

3.5. Abutment components

As shown in Fig 3.4, a spring system is established to capture the dynamic interactions of different abutment components. The numerical modelling of each abutment component is discussed in detail below.

3.5.1 Backfill

The force-displacement relationship of the backfill under passive earth pressure can be expressed by a hyperbolic model, which can be further parameterized using the following formula [45-46]:

$$F(y) = \frac{y}{\frac{1}{K_{ave}} + R_f \frac{y}{F_{ult}}} \quad (3.4)$$

$$K_{ave} = \frac{F_{ult}}{2y_{ave}} \quad (3.5)$$

where K_{ave} defines the effective stiffness of the model and is determined by the cut-line stiffness connecting the origin and 0.5 times the ultimate load, and the corresponding deformation is expressed as y_{ave} , F_{ult} is the ultimate capacity at a lateral displacement of $0.1H_{abut}$ considered in this study, H_{abut} is the abutment wall height, and R_f is the failure ratio, which can be computed as:

$$R_f = 1 - \frac{F_{ult}}{K_{ave}y_{max}} \quad (3.6)$$

Based on experimental data on retaining structures similar to bridge abutments, Shamsabadi [46] gave an empirical formula for the force-displacement curve for practical application:

$$F(y) = \frac{272.8y}{1 + 1.18y} \left(\frac{H}{1m}\right)^{1.5} \quad (sand) \quad (3.7)$$

$$F(y) = \frac{150.8y}{1 + 0.51y} \left(\frac{H}{1m}\right) \quad (clay) \quad (3.8)$$

According to the geological survey, the type of abutment backfill is clay for the A Viaduct. Moreover, the value of K_{ave} is computed as 7417434 kN/m, the R_f is taken as 0.95, the F_{ult} is taken as 276349 kN, and the hyperbolic gap material is used to simulate the backfill element in OpenSees.

3.5.2 Pounding element between abutment and deck

The Hertz contact model with a nonlinear hysteresis is used to simulate the impact pounding element, where the dissipated energy can be expressed as:

$$E = \frac{k_h \delta_m^{n+1} (1 - e^2)}{n + 1} \quad (3.9)$$

Where k_h is the impact stiffness parameter, n is the Hertz coefficient, which is typically taken as 1.5, e is the coefficient of restitution with typical values from 0.6-0.8, and δ_m is the relative penetration taken as 0.016 m. The impact stiffness, k_h , can be expressed as [47]:

$$k_h = \frac{4}{3\pi(h_1 + h_2)} \left[\frac{R_1 R_2}{R_1 + R_2} \right]^{\frac{1}{2}} \quad (3.10)$$

where h_1, h_2 are material parameters that can be computed as:

$$h_i = \frac{1 - \nu_i^2}{\pi E_i} \quad (3.11)$$

where ν_i and E_i are the Poisson's ratio and elastic modulus of sphere i . Assuming the two colliding structures as spheres, the radius of the sphere can be estimated as:

$$R_i = \sqrt[3]{\frac{3m_i}{4\pi\rho}} \quad (3.12)$$

where m_i is the colliding mass, and ρ is the density of the reinforced concrete (28kN/m³). The Impact stiffness, k_h , can then be calculated as 2.423×10^7 kN/m, where the effective stiffness, k_{eff} , of the impact element is further computed as:

$$k_{eff} = k_h \sqrt{\delta_m} \quad (3.13)$$

And the yield displacement is:

$$\delta_y = a\delta_m \quad (3.14)$$

where a is typically taken as 0.1, the initial stiffness k_1 and secondary stiffness k_2 are chosen

such that the energy dissipated by the impact model during the collision is consistent with the associated energy dissipated in the Hertz model.

$$k_1 = k_{eff} + \frac{E}{a\delta_m^2} \quad (3.15)$$

$$k_2 = k_{eff} - \frac{E}{(1-a)\delta_m^2} \quad (3.16)$$

According to the calculation, $k_1 = 9.281 \times 10^7 \text{ kN/m}$, $k_2 = 1.865 \times 10^7 \text{ kN/m}$. A hysteretic gap material is used in OpenSees to simulate the impact element.

3.5.3 Pulling bars

To simulate the effect of pulling bars, the *steel02* material is applied in OpenSees to connect the abutment and deck with the zero-length tension-only element. According to the properties of S500/600 steel, the stiffness of the steel bars is set as 777439 kN/m, and the yield force is set as 14500kN.

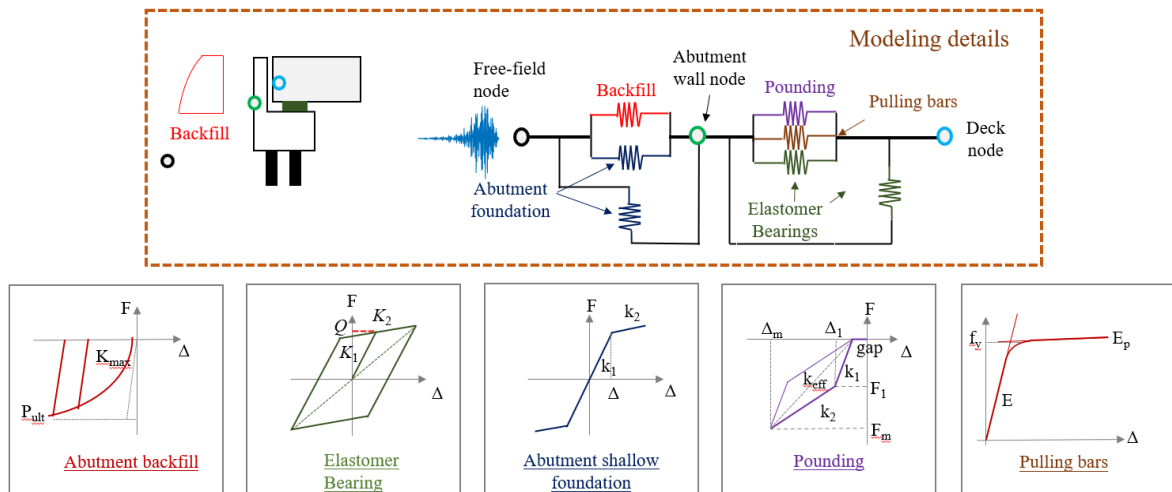


Fig 3.4 Spring System Considered for Simulating End Abutments

3.6. Foundation

As shown in Figure 2.1, two different types of foundations, pile foundations, and spread footings, are designed for the A Viaduct.

3.6.1 Pile foundation

The R5P (termed as response five parameter) model is adopted for the hysteric material in OpenSees to simulate the pile-foundation-soil system [57]. R5P model can incorporate nonlinear behaviours of soil materials, a wide array of heterogeneous soil profiles, and realistic connection details between piles and pile caps. According to the numerical modelling scheme of the pile-soil system [57] and the pile/soil properties of the A Viaduct, cyclic pushover analyses are conducted on the pile-soil system. Furthermore, the R5P model can be developed by regressing the hysteretic curves for piles at different depths [57], as shown in Fig 3.5.

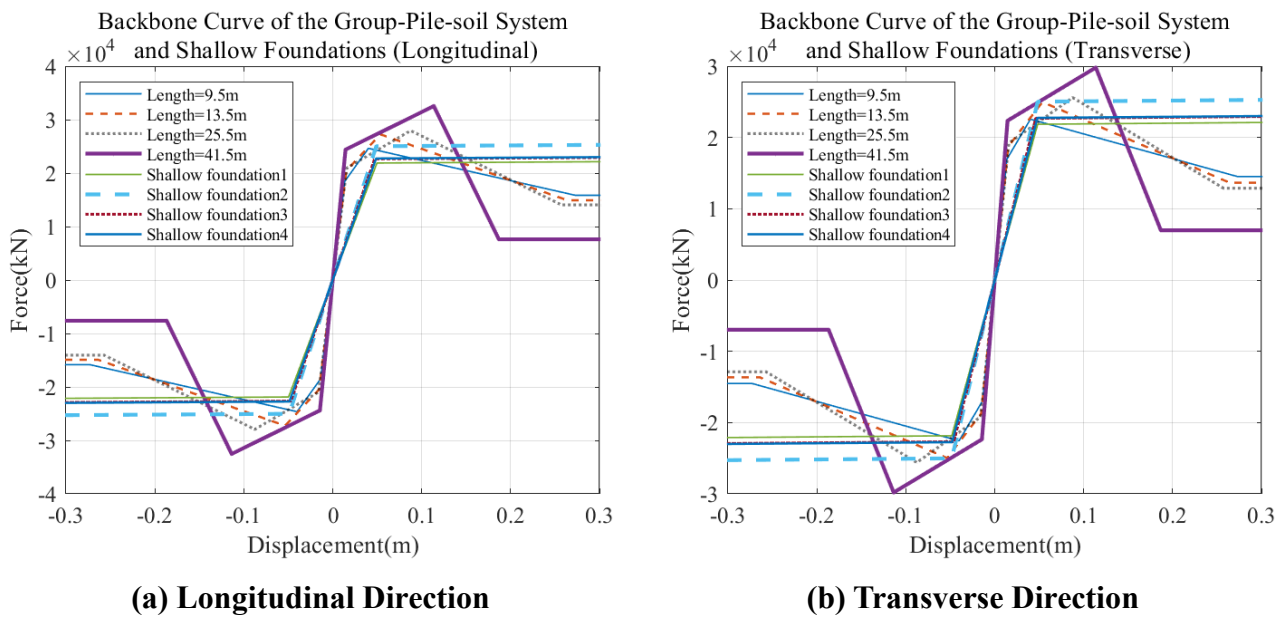


Fig 3.5 Backbone Curves of the Piles using the R5P Model and shallow foundations

Pile foundations for the A Viaduct contain arrays of multiple rows and columns of piles, whose interaction typically results in a pile group with a capacity lower than the simple sum of individual pile capacities. Since the lateral resistance of the group piles needs to be reduced, group factors f_m is applied to individual piles based on pile spacing and the number of piles per row/column. Xie et al. [57] proposed a procedure, based on Rollins et al. [58], for calculating the group amplification factor A_m , which amplifies the backbone response of a single pile to the backbone response of a group of piles. This procedure assigns the largest grouping factor value f_{m1} to the first row, the reduced value f_{m2} to the second row, and the smallest value f_{m3} is assigned to the third and all subsequent rows as follows:

$$f_m = \begin{cases} 0.26 \ln\left(\frac{S}{D}\right) + 0.5 \leq 1.0 & \text{for first row} \\ 0.52 \ln\left(\frac{S}{D}\right) \leq 1.0 & \text{for second row} \\ 0.60 \ln\left(\frac{S}{D}\right) - 0.25 \leq 1.0 & \text{for third or higher row} \end{cases} \quad (3.17)$$

where S represents the center-to-center spacing of the piles and D is the diameter of the piles.

The amplification factor can then be calculated as:

$$A_{m,x} = f_{m,x1}n_y + f_{m,x2}n_y + f_{m,x3}n_y(n_x - 2) \quad (3.18)$$

$$A_{m,y} = f_{m,y1}n_x + f_{m,y2}n_x + f_{m,y3}n_x(n_y - 2) \quad (3.19)$$

where n_x and n_y are the number of piles in longitudinal and transverse directions, respectively, $f_{m,x1}$, $f_{m,x2}$, and $f_{m,x3}$ are the group factors calculated from Eq. (3.17) for the first, second, and third rows of piles in the transverse direction, respectively; and $f_{m,y1}$, $f_{m,y2}$ and $f_{m,y3}$ are the same group factors for the piles in the transverse direction.

3.6.2 Shallow foundation

The *TzSimple2* material [59] is applied in OpenSees to simulate the lateral behaviours of shallow foundations; the material has two input parameters: the ultimate capacity t_{ult} and the displacement at which 50% of the ultimate load is mobilized z_{50} . The sliding resistance of the foundation can be calculated as:

$$t_{ult} = W_g \tan \delta + A_b C \quad (3.20)$$

where W_g is the total weight above the foundation, δ is the friction angle between the soil and the foundation, which is usually taken as 1/3 to 2/3 of the friction angle of soil, A_b is the area of the spread footing foundation, and C is the soil cohesion. Besides, z_{50} can be calculated as follows:

$$z_{50} = \frac{C_e t_{ult}}{k_{el}} \quad (3.21)$$

where C_e is the empirical coefficient that is determined by fitting the friction behaviour of shallow foundations, which is taken 0.708 for clay, and k_{el} is the elastic stiffness of the shallow foundation, which can be computed based on the suggestions from Gazetas (1991) [62] for both long side (K'_y) and short side (K'_x) of the foundation:

$$K'_y = \frac{GL}{2 - \nu} \left[2 + 2.5 \left(\frac{B}{L} \right)^{0.85} \right] \quad (3.22)$$

$$K'_x = \frac{GL}{2 - \nu} \left[2 + 2.5 \left(\frac{B}{L} \right)^{0.85} \right] + \frac{GL}{0.75 - \nu} \left[0.1 \left(1 - \frac{B}{L} \right) \right] \quad (3.23)$$

where L is the foundation length, B is the foundation width, G is the Shear Modulus of the interface soil, and ν is its Poisson's ratio.

To avoid convergence issues, the *TzSimple2* material is further simplified as an equivalent bilinear model to simulate the lateral resistances of spread footings. Figure 3.5 also compares the force-displacement relationships of four shallow foundations together with those for pile foundations.

4 Physics-based Simulations of Ground Motions at the A Viaduct

4.1. Overall methodology

Zhang et al. [63-65] investigated the influence of site-specific surface topography and soil stratigraphy on the dynamic soil-structure interaction behaviour of structures located in the southeastern European side of Istanbul city. They surveyed the geological and geotechnical data of the Istanbul city from 2912 boreholes to develop the shear wave velocity and density profiles of citywide soils at different depths. Afterwards, the major topographic features and properties of soil in the Istanbul metropolitan area were simulated by implementing a virtual topography method [66] in Hercules [67], an octree-based finite element parallel software. Finally, physics-based simulated ground motions were obtained from Central Marmara Basin (CMB) and the North Boundary Fault (NBF) using the hybrid method [68]. These simulated motions are adopted as the input ground motions in the current study. Compared with flat free-surface results (FLAT), the virtual topography method can capture the change due to the topographic irregularities and detect high-resolution topographic effects.

4.2. Selected ground motions

Six groups of simulated ground motions are selected herein, whereas each motion group contains 12 motion records at 12 column/abutment foundations for the A Viaduct. Table 4.1 gives a summary of the fault dimensions, rupture areas, and seismic moments of the 6 events included in this study, where \mathbf{A} denotes the rupture area (the product of fault length \mathbf{L} and width \mathbf{W}). The seismic moment \mathbf{M}_0 is considered as 6.31×10^{18} , which is used to calculate moment magnitude M_w according to the equation proposed by Hanks and Kanamori (1979) [69] :

$$M_w = \frac{\log M_0 - 9.1}{1.5} \quad (4.1)$$

The epicenters information (longitude, latitude and hypocentral depth \mathbf{H}) of the simulated ground motions are also listed in Table 4.1. The ground motion records of the first motion group, denoted as SIM024, are shown in Table 4.2; information regarding all other ground

motion records is listed in Appendix A.

As shown in Table 4.2, the Peak Ground Accelerations (PGAs) indicate significant variances across the 12 foundation motions for exciting the bridge. The response spectra and time histories of the 12 ground motions are shown in Figs 4.1 and 4.2, respectively. Fig 4.1 indicates that large variances of the twelve motions occur in the response spectra for periods up to 1 second. At the natural period of the A Viaduct (i.e., 4.07 s), response spectra of the twelve motions show minor differences, which is consistent with the results shown in Table 4.2. The time-history comparison in Fig 4.2 also confirms the overall high-frequency nature of the simulated ground motions. It remains interesting to observe how these twelve motions would change the time-history responses of the A Viaduct.

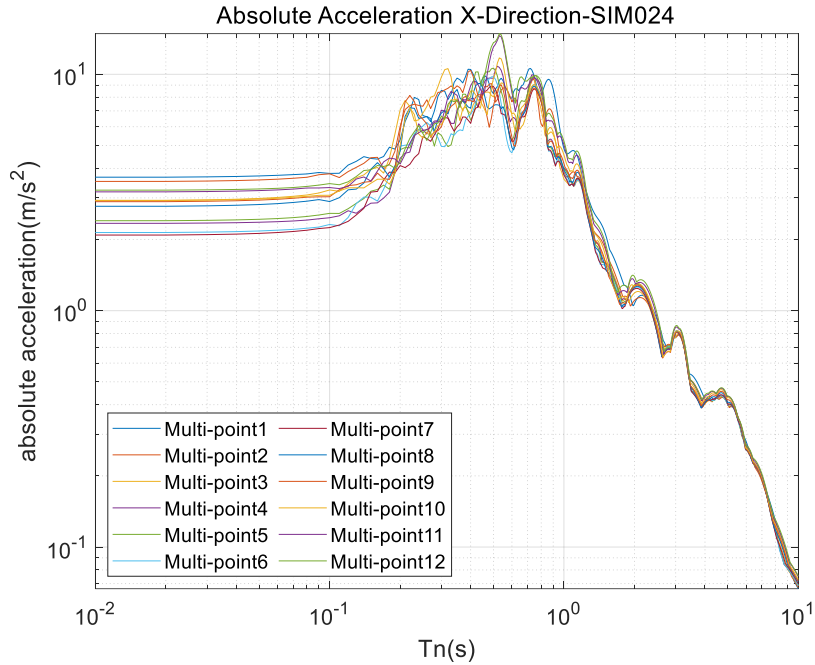
Table 4.1 Parameters of Simulation Ground Motions

Simulation	Mw	M ₀ (N·m)	L (km)	W (km)	A (km ²)	Lon (°)	Lat (°)	D (km)
SIM023	6.49	6.31×10 ¹⁸	27.5	11	302.5	28.9167	40.8633	8.5
SIM024	6.49	6.31×10 ¹⁸	27.5	11	302.5	29.0473	40.8011	8.5
SIM025	6.49	6.31×10 ¹⁸	27.5	11	302.5	29.1776	40.7387	8.5
SIM026	6.49	6.31×10 ¹⁸	27.5	11	302.5	28.8931	40.8347	7.5
SIM027	6.49	6.31×10 ¹⁸	27.5	11	302.5	29.0237	40.7725	7.5
SIM028	6.49	6.31×10 ¹⁸	27.5	11	302.5	29.1539	40.7102	7.5

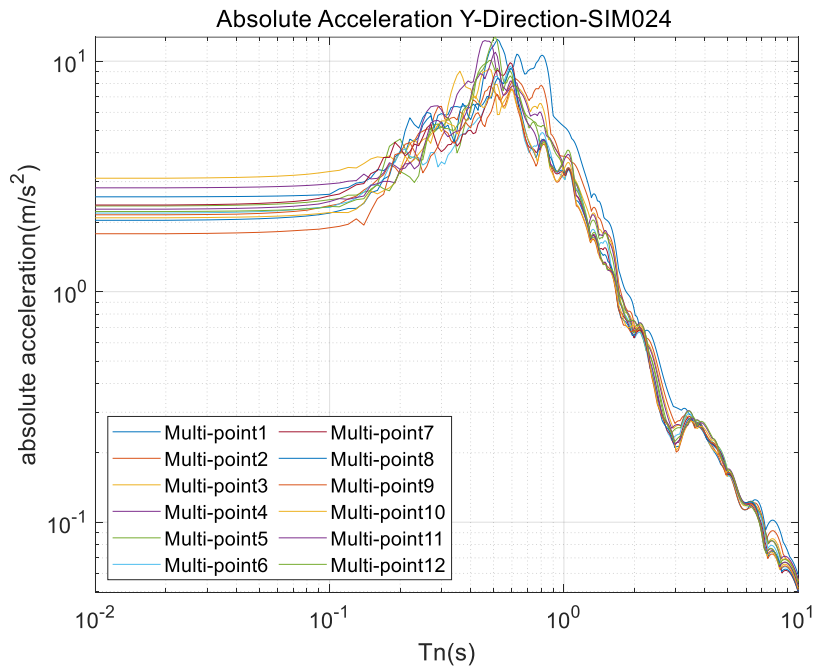
Table 4.2 Ground Motion Records for Group SIM024

Input Foundation	Station	Direction	PGA (cm/s ²)	Sa (4.07s) (cm/s ²)	Direction	PGA (cm/s ²)	Sa (4.07s) (cm/s ²)
Ab1	1	X	367	42	Y	258	24
P1	2	X	352	41	Y	216	24
P2	3	X	293	41	Y	311	23
P3	4	X	234	42	Y	282	23
P4	5	X	240	42	Y	235	23
P5	6	X	214	42	Y	219	23
P6	7	X	209	41	Y	238	23
P7	8	X	276	42	Y	204	23
P8	9	X	289	42	Y	178	24

P9	10	X	293	43	Y	209	25
P10	11	X	318	44	Y	228	26
Ab2	12	X	324	45	Y	223	26

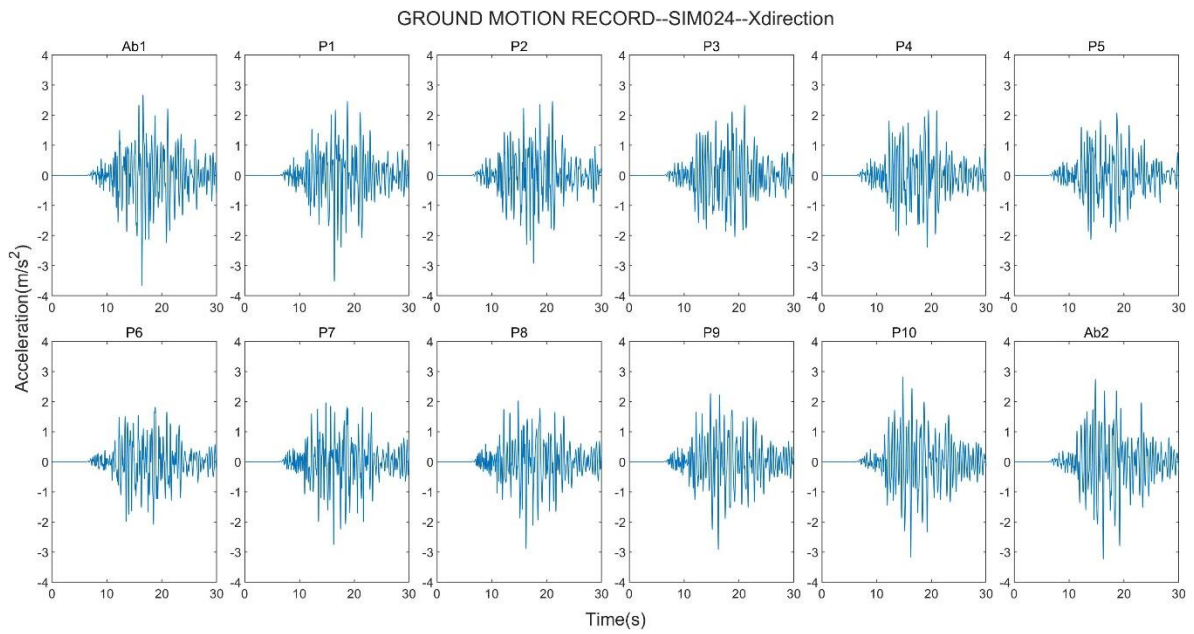


(a) Longitudinal Direction

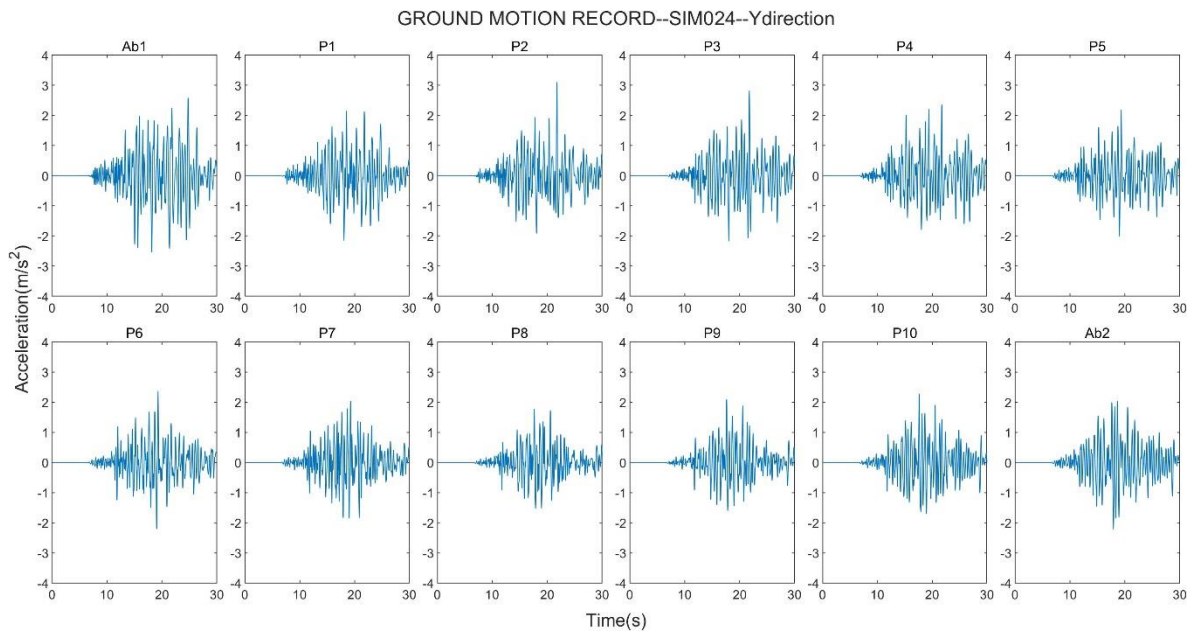


(b) Transverse Direction

Fig 4.1 Response Spectra of the Selected Twelve Ground Motions



(a) Longitudinal Direction



(b) Transverse Direction

Fig 4.2 Acceleration Time Histories of the Selected Twelve Ground Motions

5. Seismic Response Analyses of the A Viaduct Under Different Motion Inputs

The A viaduct is excited by two different ground motion excitation schemes – the uniform excitation, where each bridge foundation is applied with the same motion, and the multi-support excitation, where different motions from 1-12 are applied individually to the corresponding column/abutment foundations in both longitudinal and transverse directions. The input motions to the numerical model will cause different bridge components to respond differently in time histories. The responses of these components under both uniform and multi-support excitations are compared and discussed in this chapter.

5.1. Uniform excitation

By taking the geometric mean of the motions in longitudinal and transverse directions, the group motions with the maximum and minimum PGAs are identified. As such, the uniform excitation scheme considers two motion cases – the maximum case where the largest PGA motions among the 12 motions are used to excite the A Viaduct at all foundations and the minimum case where the smallest PGA motions are used.

5.2. Multi-support excitation

The multiple support excitations are input in the form of acceleration waves in OpenSees. Therefore, twelve acceleration time histories of seismic ground motions are used to excite the twelve supporting foundations of the A Viaduct simultaneously.

5.3. Response comparisons of critical bridge components

5.3.1 Column

Table 5.1 summarizes the peak displacements of the 10 columns under uniform and multiple support excitations. In the table, “Max” denotes the use of the maximum motion inputs in uniform excitation; “Min” represents the use of the minimum motion inputs; “Multi” indicates the multi-support excitation scheme that has different motions applied to different foundation input points. Besides, “L” and “T” represent the column’s longitudinal and transverse responses, respectively. In the longitudinal direction, the multi-support excitation scheme captures the peak column displacement of 20.9 cm at Column P9, which is close to the one from the

maximum motion case (i.e., 18.5 cm at Column P9). Likewise, similar longitudinal responses can be observed between multi-support and maximum motions for Columns P1, P2, P3, P4, P8, P9, and P10. However, this is not the case for the remaining columns, where significant differences can be observed. For instance, the longitudinal displacement of Column P7 under the multi-support excitation is 9.4 cm; the displacement for the same column is increased to 19.5 cm when the maximum motions are used. Generally, the maximum motion case tends to overestimate column displacements, while the minimum motion case shows the smallest displacements for about half of the columns. Smaller displacement responses can be observed for the columns in the transverse direction. As a result, these three motion excitation schemes show closer column responses in this direction.

Table. 5.1 The Peak Displacements of Columns under Uniform/Multi-support Excitations (unit: cm)

Column	Case	Displacement		Column	Case	Displacement	
		L	T			L	T
P1	Max	13.1	12.0	P6	Max	1.1	0.7
	Min	9.4	8.9		Min	0.7	0.6
	Multi	12.5	11.1		Multi	0.7	0.7
P2	Max	3.1	2.1	P7	Max	19.5	9.3
	Min	2.5	2.0		Min	10.2	11.3
	Multi	2.8	2.1		Multi	9.4	9.7
P3	Max	2.3	1.4	P8	Max	8.9	5.4
	Min	1.9	1.3		Min	9.1	4.2
	Multi	2.0	1.3		Multi	8.8	4.3
P4	Max	1.7	0.9	P9	Max	20.9	7.0
	Min	1.4	0.8		Min	16.7	6.7
	Multi	1.4	0.8		Multi	18.5	7.5
P5	Max	1.4	1.0	P10	Max	19.6	5.5
	Min	0.9	0.8		Min	15.8	6.5
	Multi	0.9	0.8		Multi	19.3	7.3

To better illustrate the responses of columns under three cases of excitations, Fig 5.1 shows the hysteretic curves of three representative columns – P1, P7, and P9, in the longitudinal direction. As shown in the figure, all three columns enter the nonlinear phases with substantial hysteretic loops. In particular, different excitation schemes have produced column force-displacement responses that significantly differ from each other.

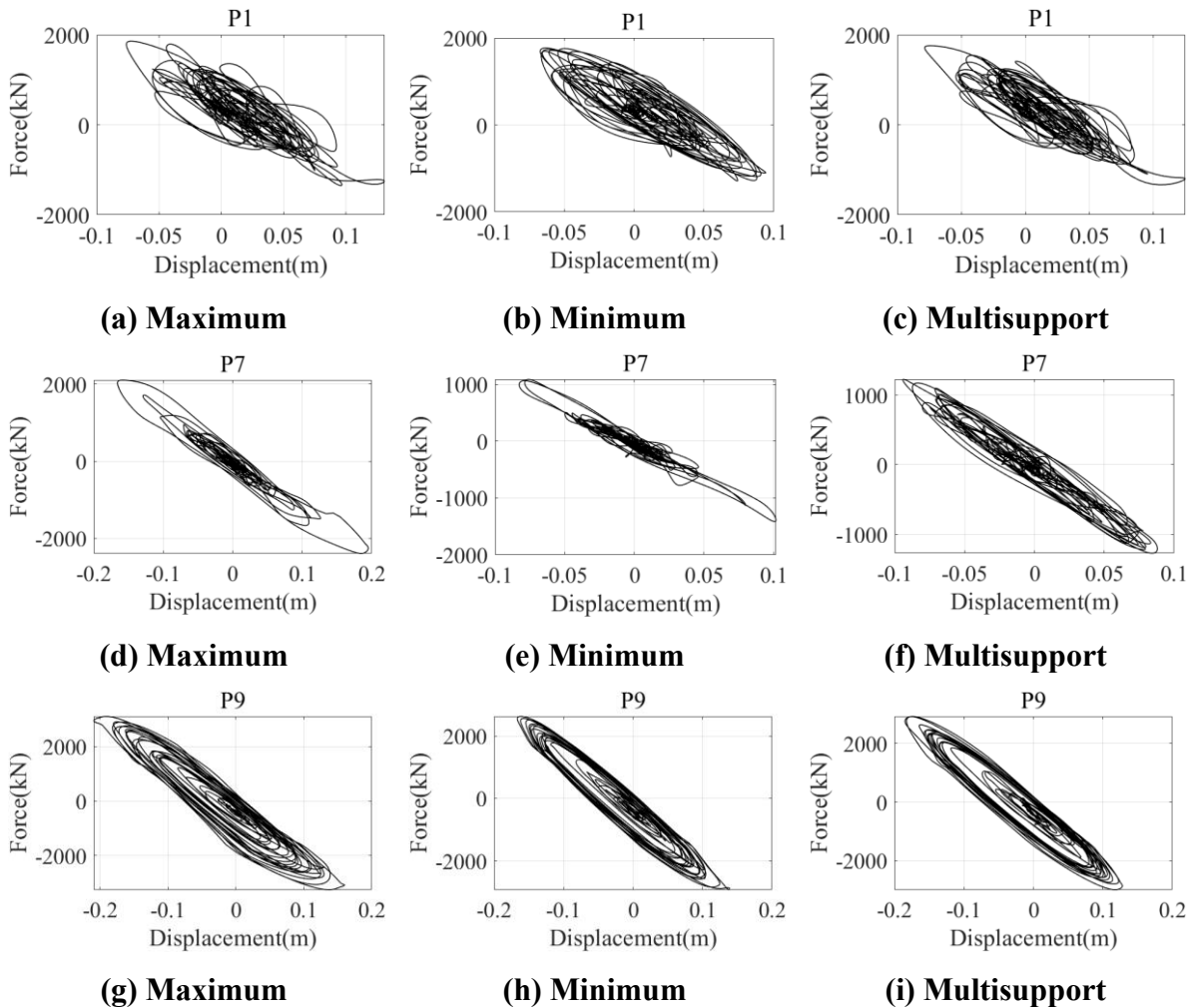


Fig 5.1 Hysteretic Curves of Piers under Different Excitation Schemes

5.3.2 Bearing

The peak displacements of all bearings are compared in Table 5.2 when the A Viaduct is subjected to the three motion excitation schemes. As highlighted, bearings at Columns P4, P5, P7, and P9 show significant differences in displacement responses. In particular, the longitudinal bearing displacement at Column P5 is overestimated by about 50% (i.e., from 7.1

cm to 10.5 cm) should the maximum uniform excitation motions be used as the inputs. Similar conclusions can be drawn for the bearing displacement in the transverse direction, where the maximum uniform excitation changes the bearing displacement at Column P3 from 14.1 cm to 17.1 cm. By contrast, the minimum uniform excitation motions show the overall smallest peak bearing displacements, and the largest difference occurs in Column P7, where the bearing displacement in the longitudinal direction is reduced from 11.4 cm to 8.8 cm.

Table 5.2 The Peak Displacements of Bearings under Uniform and Multi-support Excitations (unit: cm)

Bearing	Case	Displacement		Bearing	Case	Displacement	
		L	T			L	T
P1	Max	11.2	7.4	P6	Max	11.3	12.4
	Min	10.8	4.6		Min	6.8	16.0
	Multi	10.5	4.8		Multi	8.0	14.6
P2	Max	6.1	14.4	P7	Max	15.0	10.2
	Min	3.4	12.4		Min	8.8	11.5
	Multi	4.4	12.7		Multi	11.4	9.6
P3	Max	6.0	17.1	P8	Max	15.2	8.8
	Min	4.7	13.8		Min	18.3	5.5
	Multi	5.8	14.1		Multi	19.2	6.7
P4	Max	7.5	12.2	P9	Max	27.9	6.0
	Min	5.2	11.5		Min	22.5	3.9
	Multi	6.2	11.0		Multi	23.5	5.0
P5	Max	10.5	11.3	P10	Max	25.8	4.2
	Min	6.2	13.6		Min	20.0	4.2
	Multi	7.1	13.5		Multi	24.2	5.6

Figure 5.2 shows the force-displacement hysteretic curves for three representative bearings (i.e., P4, P5, and P9) under different excitation schemes, where Figure 5.2 (a)-(c) shows the bearing responses in the transverse direction and the remaining figures indicate the longitudinal responses. It is evident that the maximum-motion uniform excitation case tends to

overestimate bearing responses. Both bearings P4 and P9 show nonlinear behaviours under the multi-support excitation scheme.

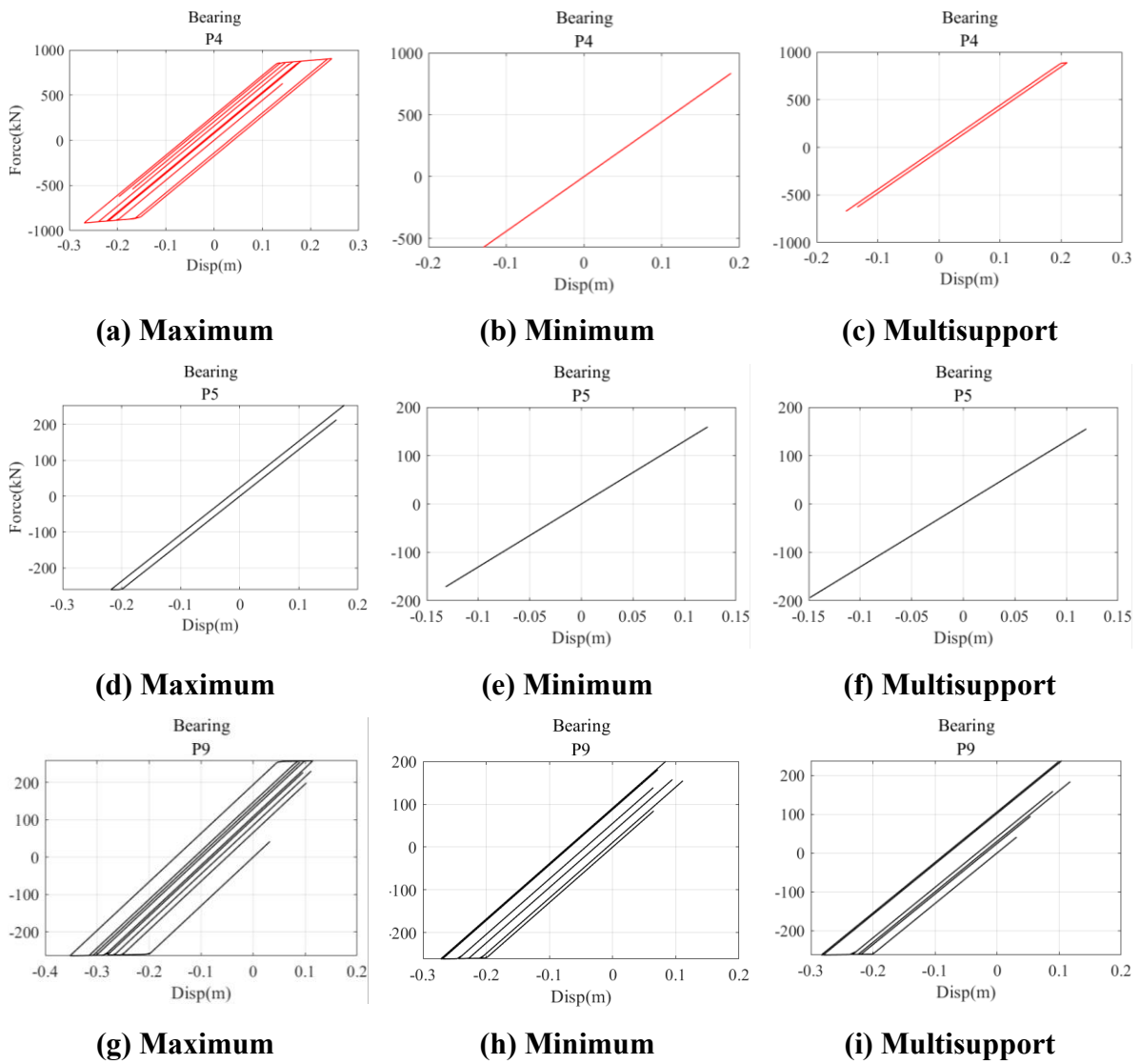
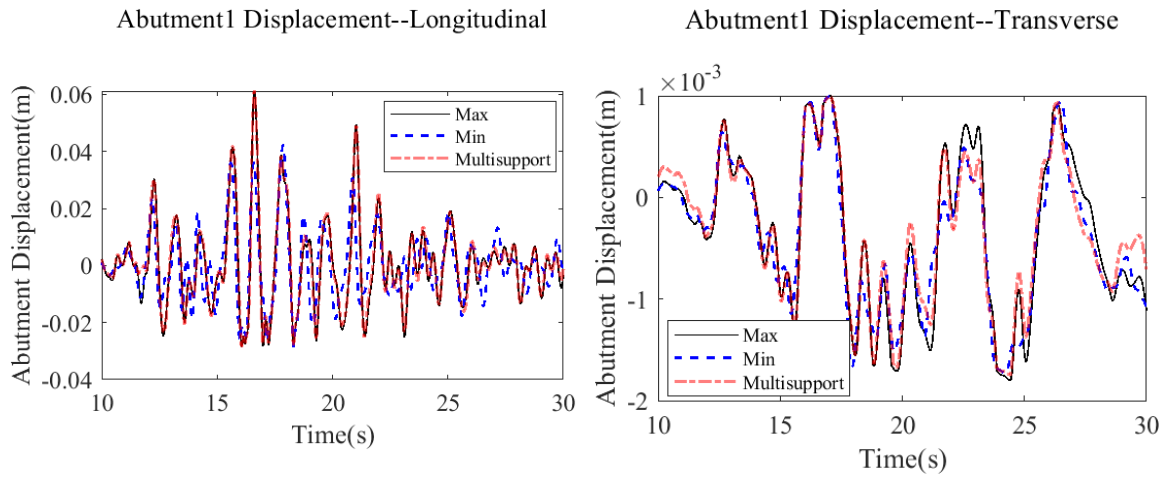
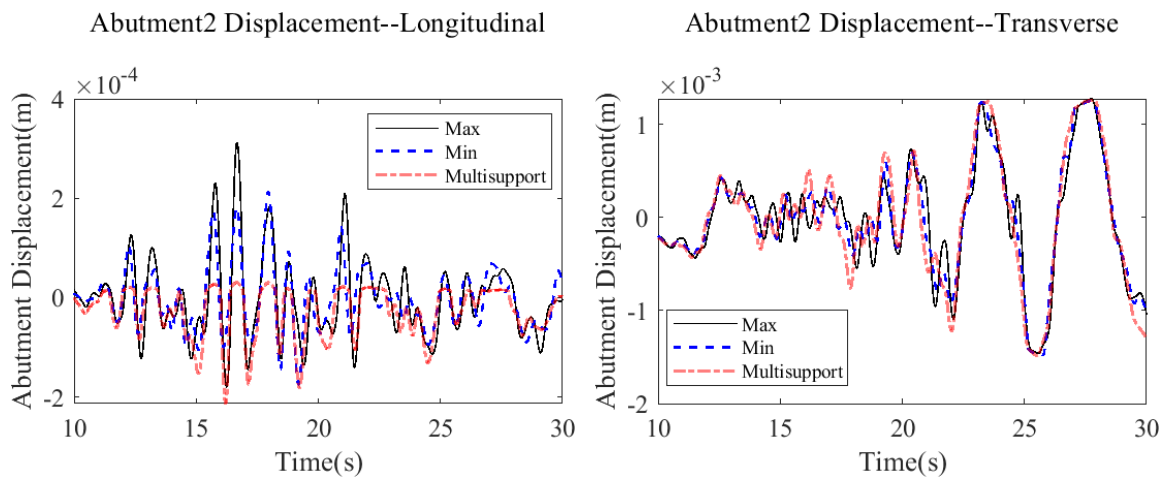


Fig 5.2 Hysteretic Curves for Representative Bearings under Different Excitations

5.3.3 Abutment



(a) Displacement of the West Abutment

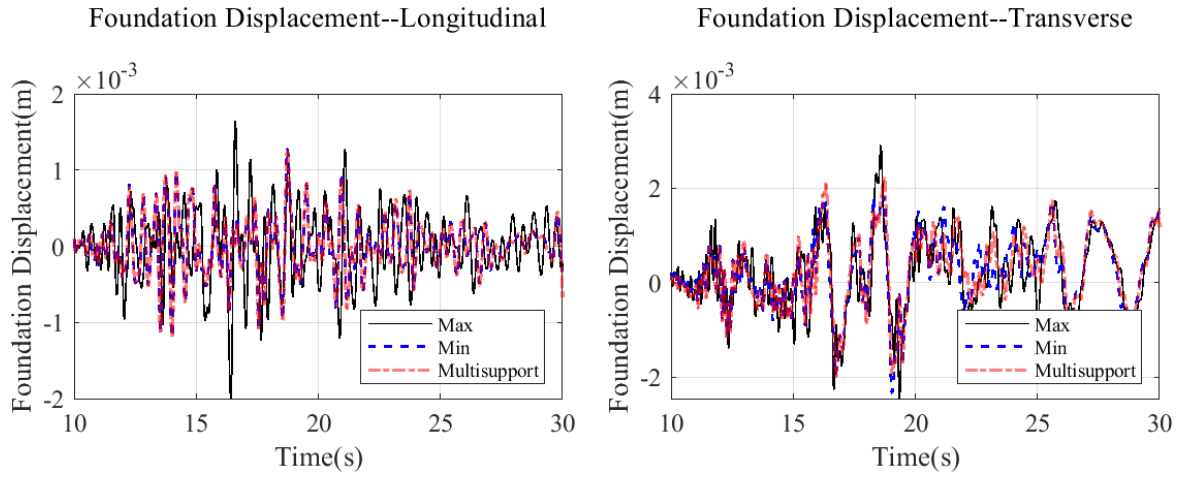


(b) Displacement of the East Abutment

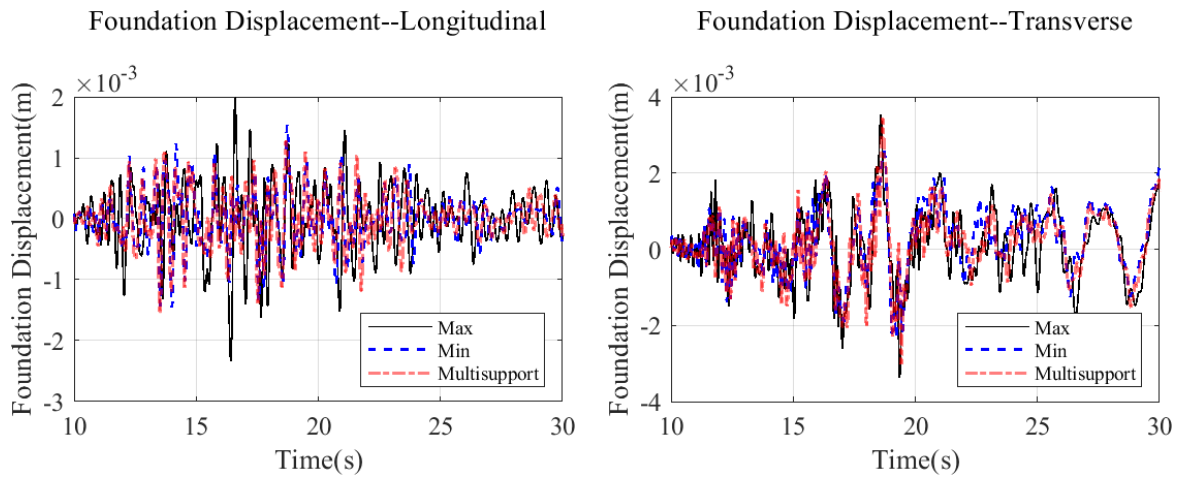
Fig 5.3 Displacement Time Histories of End Abutments

The time-history curves of nodal displacement of abutments under different excitation methods are provided in Fig 5.3. For the abutments under maximum-motion uniform excitations, the maximum nodal displacement of the west and east abutments are 5.98 cm and 0.19 cm, respectively. When it comes to the vibration under multi-support excitations, the maximum displacements of west and east abutments are 6.12 cm and 0.19 cm, respectively. The maximum displacement of the west abutment is reduced substantially when the minimum-motion uniform excitations are the case scenario.

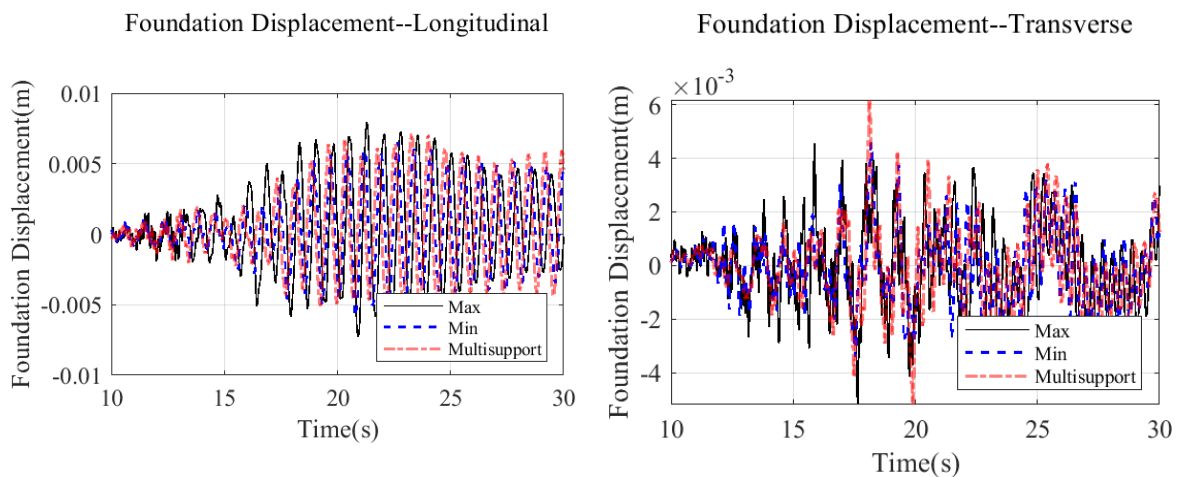
5.3.3 Foundation



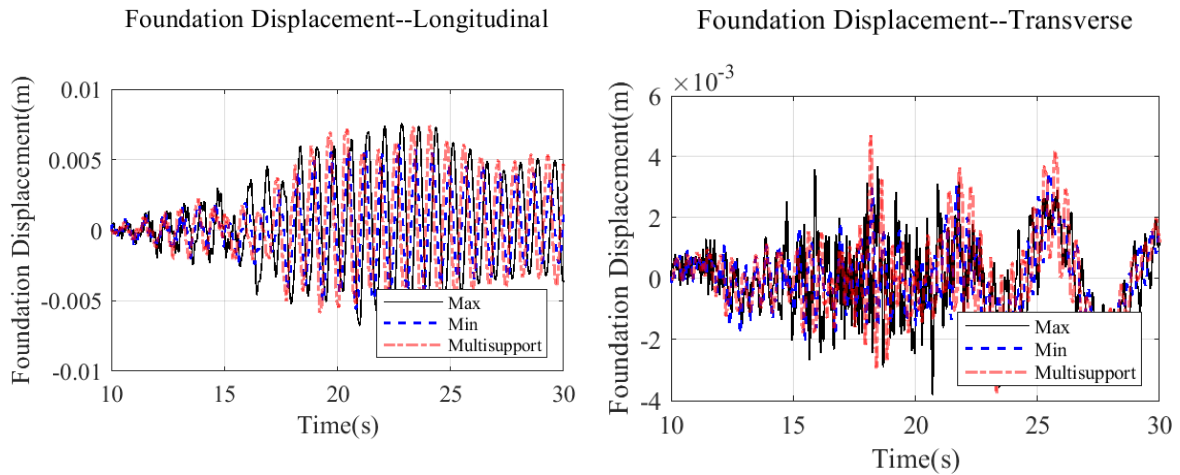
(a) Foundation 5 (Pile Foundation)



(b) Foundation 6 (Pile Foundation)



(c) Foundation 9 (Shallow Foundation)



(d) Foundation 10 (Shallow Foundation)

Fig 5.4 Displacement Time History Curve of Foundation

Fig 5.4 compares the time history responses of foundation displacements under three excitation schemes for foundations P5, P6, P9, and P10. P5 and P6 are pile foundations, and P9 and P10 are shallow foundations. The comparisons for foundation displacements also indicate that the maximum-motion uniform excitations case would have the largest foundation displacements, followed by the multi-support excitation scheme. In contrast, the foundation displacements are reduced further when the minimum-motion uniform excitations are the input case. Comparing the displacement demand with the R5P pile capacity models also shows that all piles will be in the elastic damage without having any damage under the given set of input motions.

6. Conclusion

This thesis conducts the time history analyses of the A Viaduct, a multi-span curved continuous box-girder viaduct in Istanbul, Turkey, under different schemes of ground motion excitations. The software platform of OpenSees is used to build the 3D nonlinear finite element model for the viaduct; 12 sets of simulated ground motions considering the topographic effect at the bridge site are used for uniform excitations and multiple support excitations, respectively. Seismic responses of the A Viaduct under additional sets of ground motions are provided in the Appendix, where similar observations can be pinpointed. The following conclusions can be drawn from the current work:

1. The literature review indicates the importance of using multiple support excitation to capture the topographic effect in ground motion inputs.
2. The numerical model developed in OpenSees indicates the nonlinear dynamic interactions among various bridge components, including column, bearing, foundation, and abutment components (impact element, backfill, pull bars, etc.)
3. Under the given set of ground motions, both columns and bearings show nonlinear behaviours.
4. Among the chosen three motion excitation schemes, the multi-support excitation scheme bears the most promising strategy to capture the responses of different bridge components reliably. However, the maximum-motion uniform excitation scheme tends to overestimate bridge responses, while the minimum-motion uniform excitation shows the smallest responses in many cases.

This thesis focused on the effect of multi-support excitation and uniform excitation on the seismic performance of A Viaduct. However, there exist additional problems that remain unsolved; potential future works can be:

1. Many more sets of ground motions should be included in future analyses to cover more physics-based earthquake scenarios.
2. Seismic fragility and risk assessment should be conducted on the A Viaduct to transparently and comprehensively evaluate the soundness of the multi-support excitation scheme.

Reference

- [1] Linzell, D., R. T. Leon, and A. H. Zureick. "Experimental and analytical studies of a horizontally curved steel I-girder bridge during erection." *Journal of Bridge Engineering* 9.6 (2004): 521-530.
- [2] Abbasi, Mohammad, et al. "Seismic vulnerability assessment of a Californian multi-frame curved concrete box girder viaduct using fragility curves." *Structure and Infrastructure Engineering* 12.12 (2016): 1585-1601.
- [3] Makris, Nicos, M. C. Constantinou, and G. F. Dargush. "Analytical model of viscoelastic fluid dampers." *Journal of Structural Engineering* 119.11 (1993): 3310-3325.
- [4] Iwasaki, Toshio, Ray W. Clough, and Joseph Penzien. *Literature survey-Seismic effects on highway bridges*. Earthquake Engineering Research Center, College of Engineering, University of California, 1972.
- [5] Singh, Mahendra P., and Luis M. Moreschi. "Optimal placement of dampers for passive response control." *Earthquake engineering & structural dynamics* 31.4 (2002): 955-976.
- [6] Lu G C, Hu L T. "Analysis of Parametric Sensitivity of Fluid Viscous Dampers for Xihoumen Bridge." *World Bridges* 2 (2005): 43-45.
- [7] Ou J P, Ding J H. "Theory and Performance Experiment of Viscous Damper of Clearance Hydrocylinder." *Earthquake Engineering and Engineering Vibration* 19.4 (1999): 82-89.
- [8] Crouse, C. B., B. Hushmand, and G. R. Martin. "Dynamic soil–structure interaction of a single - span bridge." *Earthquake engineering & structural dynamics* 15.6 (1987): 711-729.
- [9] Werner, S. D., J. L. Beck, and M. B. Levine. "Seismic response evaluation of Meloland Road Overpass using 1979 Imperial Valley earthquake records." *Earthquake engineering & structural dynamics* 15.2 (1987): 249-274.
- [10] McCallen, David B., and Karl M. Romstad. "Dynamic analyses of a skewed short-span, box-girder overpass." *Earthquake spectra* 10.4 (1994): 729-755.
- [11] Kappos, A. J., G. D. Manolis, and I. F. Moschonas. "Seismic assessment and design of R/C bridges with irregular configuration, including SSI effects." *Engineering Structures* 24.10 (2002): 1337-1348.
- [12] Newmark, Nathan M. "Problem in wave propagation in soil and rock." *Proceedings of Int. Symp.*

Wave Propagation and Dynamic Properties of Earth Materials. Univ. New Mexico Press, 1968.

- [13] Kuesel, Thomas R. "Earthquake design criteria for subways." *Journal of the structural division* 95.6 (1969): 1213-1231.
- [14] Lamb, Horace. "I. On the propagation of tremors over the surface of an elastic solid." *Philosophical Transactions of the Royal Society of London. Series A, Containing papers of a mathematical or physical character* 203.359-371 (1904): 1-42.
- [15] Reissner, E. "Stationäre, axialsymmetrische, durch eine schüttelnde Masse erregte Schwingungen eines homogenen elastischen Halbraumes." *Ingenieur-Archiv* 7.6(1936):381-396.
- [16] Arnold, R. N., G. N. Bycroft, and G. B. Warburton. "Forced vibrations of a body on an infinite elastic solid." (1955): 391-400.
- [17] Lysmer, J. F. E. R., and F. E. Richart Jr. "Dynamic response of footings to vertical loading." *Journal of the Soil Mechanics and Foundations Division* 92.1 (1966): 65-91.
- [18] Bycroft, GoN. "Forced vibrations of a rigid circular plate on a semi-infinite elastic space and on an elastic stratum." *Philosophical Transactions of the Royal Society of London. Series A, Mathematical and Physical Sciences* 248.948 (1956): 327-368.
- [19] Zaman, Md Musharraf-uz, Chandrakant S. Desai, and Eric C. Drumm. "Interface model for dynamic soil-structure interaction." *Journal of Geotechnical Engineering* 110.9 (1984): 1257-1273.
- [20] Wolf, John P., and Pius Oberhuber. "Nonlinear soil - structure - interaction analysis using green's function of soil in the time domain." *Earthquake engineering & structural dynamics* 13.2 (1985): 213-223.
- [21] Matthees, Wolfgang, and Götz Magiera. "A sensitivity study of seismic structure-soil-structure interaction problems for nuclear power plants." *Nuclear Engineering and Design* 73.3 (1982): 343-363.
- [22] Ahmed, K. M., and A. S. Ranshi. "Dynamic response of nuclear power plant due to earthquake and aircraft impact including effect of soil-structure interaction." *Journal of Sound and Vibration* 59.3 (1978): 423-440.
- [23] Kodama, Noriko, and Kazuhito Komiya. "Model Experiment and Numerical Modelling of Dynamic Soil-Structure Interaction." *Materials with Complex Behaviour*. Springer, Berlin, Heidelberg, 2010. 269-276.

- [24] Bernat, S., and B. Cambou. "Soil-structure interaction in shield tunnelling in soft soil." *Computers and Geotechnics* 22.3-4 (1998): 221-242.
- [25] Weissman, Karen, and Jean H. Prevost. "Results and analysis of soil - structure interaction experiments performed in the centrifuge." *Earthquake engineering & structural dynamics* 20.3 (1991): 259-274.
- [26] Gutierrez, Jorge A., and Anil K. Chopra. "A substructure method for earthquake analysis of structures including structure - soil interaction." *Earthquake Engineering & Structural Dynamics* 6.1 (1978): 51-69.
- [27] Çelebi, Erkan, Fatih Göktepe, and N. Karahan. "Nonlinear finite element analysis for prediction of seismic response of buildings considering soil-structure interaction." *Natural hazards and earth system sciences* 12.11 (2012): 3495-3505.
- [28] Pak, R. Y. S., and B. B. Guzina. "Seismic soil-structure interaction analysis by direct boundary element methods." *International Journal of Solids and Structures* 36.31-32 (1999): 4743-4766.
- [29] Sato, Toshiaki, Robert W. Graves, and Paul G. Somerville. "Three-dimensional finite-difference simulations of long-period strong motions in the Tokyo metropolitan area during the 1990 Odawara earthquake (MJ 5.1) and the great 1923 Kanto earthquake (MS 8.2) in Japan." *Bulletin of the Seismological society of America* 89.3 (1999): 579-607.
- [30] Earthquake Engineering Committee of the Japan Society of Civil Engineers. *Earthquake Resistant Design for Civil Engineering Structure in Japan*. JSCE, (1992):189-260
- [31] Bard, Pierre-Yves, and Brian E. Tucker. "Underground and ridge site effects: a comparison of observation and theory." *Bulletin of the seismological Society of America* 75.4 (1985): 905-922.
- [32] Geli, Louis, Pierre-Yves Bard, and Béatrice Jullien. "The effect of topography on earthquake ground motion: a review and new results." *Bulletin of the Seismological Society of America* 78.1 (1988): 42-63.
- [33] Lichu F, *Seismic Design of Bridge*. Tong Ji UP, 1997
- [34] Wang L, Zhao C G, Wang Z F. "Seismic responses analysis of continuous rigid-framed bridge with high piers considering topographic effects and multi-support excitations." *China Civil Engineering Journal* 01(2006): 50-53,59
- [35] Bogdanoff, J. L., J. E. Goldberg, and A. J. Schiff. "The effect of ground transmission time on the

- response of long structures." *Bulletin of the Seismological Society of America* 55.3 (1965): 627-640.
- [36] Soyluk, K. "Comparison of random vibration methods for multi-support seismic excitation analysis of long-span bridges." *Engineering Structures* 26.11 (2004): 1573-1583.
- [37] Su, Liang, Shi Lin Dong, and Shiro Kato. "A new average response spectrum method for linear response analysis of structures to spatial earthquake ground motions." *Engineering structures* 28.13 (2006): 1835-1842.
- [38] Su, Liang, Shilin Dong, and Shiro Kato. "Seismic design for steel trussed arch to multi-support excitations." *Journal of Constructional Steel Research* 63.6 (2007): 725-734.
- [39] Burdette, Nicholas J., et al. "Effect of asynchronous earthquake motion on complex bridges. I: methodology and input motion." *Journal of Bridge Engineering* 13.2 (2008): 158-165.
- [40] Alexander, Nicholas A. "Multi-support excitation of single span bridges, using real seismic ground motion recorded at the SMART-1 array." *Computers & structures* 86.1-2 (2008): 88-103.
- [41] Jia, Hong-Yu, et al. "Local site effects on a high-pier railway bridge under tridirectional spatial excitations: nonstationary stochastic analysis." *Soil Dynamics and Earthquake Engineering* 52 (2013): 55-69.
- [42] Bowles, Joseph E. *Foundation analysis and design*. 1988.
- [43] Aviram, Ady, Kevin Rory Mackie, and Božidar Stojadinović. *Guidelines for nonlinear analysis of bridge structures in California*. Pacific earthquake engineering research center, 2008.
- [44] Yassin, Mohd Hisham Mohd. *Nonlinear analysis of prestressed concrete structures under monotonic and cyclic loads*. Diss. University of California, Berkeley, 1994.
- [45] Duncan, J. Michael, and Robert L. Mokwa. "Passive earth pressures: theories and tests." *Journal of Geotechnical and Geoenvironmental Engineering* 127.3 (2001): 248-257.
- [46] Shamsabadi, Anoosh, Kyle M. Rollins, and Mike Kapuskar. "Nonlinear soil–abutment–bridge structure interaction for seismic performance-based design." *Journal of geotechnical and geoenvironmental engineering* 133.6 (2007): 707-720.
- [47] Griffin, K. H. "Impact: The Theory and Physical Behaviour of Colliding Solids. W. Goldsmith. Arnold, London. 1960. 379 pp. Diagrams. 90s." *The Aeronautical Journal* 65.606 (1961): 443-443.
- [48] Davis, R. O. "Pounding of buildings modelled by an impact oscillator." *Earthquake engineering &*

- structural dynamics* 21.3 (1992): 253-274.
- [49]Chau, Kam Tim, and X. X. Wei. "Pounding of structures modelled as nonlinear impacts of two oscillators." *Earthquake engineering & structural dynamics* 30.5 (2001): 633-651.
- [50]Muthukumar, Susendar, and Reginald DesRoches. "A Hertz contact model with nonlinear damping for pounding simulation." *Earthquake engineering & structural dynamics* 35.7 (2006): 811-828.
- [51]Mazzoni, Silvia, et al. "OpenSees command language manual." *Pacific Earthquake Engineering Research (PEER) Center* 264 (2006): 137-158.
- [52]Scott, Bryan D., Robert Park, and Michael JN Priestley. "Stress-strain behavior of concrete confined by overlapping hoops at low and high strain rates." *Journal Proceedings*. Vol. 79. No. 1. 1982.
- [53]Filippou, Filip C., Egor Paul Popov, and Vitelmo Victorio Bertero. "Effects of bond deterioration on hysteretic behavior of reinforced concrete joints." (1983): 137-147.
- [54]Xie, Yazhou, and Jian Zhang. "Optimal design of seismic protective devices for highway bridges using performance-based methodology and multiobjective genetic optimization." *Journal of Bridge Engineering* 22.3 (2017): 04016129.
- [55]Wolf, John P. *Foundation vibration analysis using simple physical models*. Pearson Education, 1994.
- [56]Mylonakis, George, et al. *Development of analysis and design procedures for spread footings*. Multidisciplinary Center for Earthquake Engineering Research, 2002.
- [57]Xie, Yazhou, et al. "Probabilistic seismic response and capacity models of piles for statewide bridges in California." *Journal of Structural Engineering* 147.9 (2021): 04021127.
- [58]Rollins, Kyle M., et al. "Pile spacing effects on lateral pile group behavior: Analysis." *Journal of geotechnical and geoenvironmental engineering* 132.10 (2006): 1272-1283.
- [59]Raychowdhury, Prishati, and Tara C. Hutchinson. "ShallowFoundationGen OpenSees Documentation." *Open System for Earthquake Engineering Simulation (OpenSEES): University of California, San Diego* (2008).
- [60]Gazetas, George. "Formulas and charts for impedances of surface and embedded foundations." *Journal of geotechnical engineering* 117.9 (1991): 1363-1381.
- [61]Makris, Nicos, and George Gazetas. "Dynamic pile - soil - pile interaction. Part II: Lateral and

- seismic response." *Earthquake engineering & structural dynamics* 21.2 (1992): 145-162.
- [62] Gazetas, George. "Foundation vibrations." *Foundation engineering handbook*. Springer, Boston, MA, 1991. 553-593.
- [63] Zhang, W., et al. "An investigation of the effects of surface topography on the seismic structural demands for a region of Istanbul." *Earthquake Geotechnical Engineering for Protection and Development of Environment and Constructions*. CRC Press, 2019. 5873-5880.
- [64] Zhang, Wenyang, et al. "A computational workflow for rupture - to - structural - response simulation and its application to Istanbul." *Earthquake Engineering & Structural Dynamics* 50.1 (2021): 177-196.
- [65] Zhang, W., et al. "An investigation of the effects of surface topography on the seismic structural demands for a region of Istanbul." *Earthquake Geotechnical Engineering for Protection and Development of Environment and Constructions*. CRC Press, 2019. 5873-5880.
- [66] Restrepo, Doriam, and Jacobo Bielak. "Virtual topography: A fictitious domain approach for analyzing free - surface irregularities in large - scale earthquake ground motion simulation." *International Journal for Numerical Methods in Engineering* 100.7 (2014): 504-533.
- [67] Tu, Tiankai, et al. "From mesh generation to scientific visualization: An end-to-end approach to parallel supercomputing." *SC'06: Proceedings of the 2006 ACM/IEEE conference on Supercomputing*. IEEE, 2006.
- [68] Ansal, Atilla, et al. "Loss estimation in Istanbul based on deterministic earthquake scenarios of the Marmara Sea region (Turkey)." *Soil Dynamics and Earthquake Engineering* 29.4 (2009): 699-709.
- [69] Hanks, Thomas C., and Hiroo Kanamori. "A moment magnitude scale." *Journal of Geophysical Research: Solid Earth* 84.B5 (1979): 2348-2350.
- [70] Bielak, Jacobo, et al. "Domain reduction method for three-dimensional earthquake modeling in localized regions, Part I: Theory." *Bulletin of the seismological Society of America* 93.2 (2003): 817-824.
- [71] Kaneko, Yoshihiro, et al. "Ultra - long duration of seismic ground motion arising from a thick, low - velocity sedimentary wedge." *Journal of Geophysical Research: Solid Earth* 124.10 (2019): 10347-10359.

Appendix A – All Sets of Ground Motion Records

Table A.1 Ground Motion Records - SIM23

Station	Direction	PGA (cm/s ²)	Sa (4.07s) (cm/s ²)	Direction	PGA (cm/s ²)	Sa (4.07s) (cm/s ²)
1	X	126	7	Y	93	5
2	X	101	5	Y	95	5
3	X	92	5	Y	81	5
4	X	93	5	Y	115	5
5	X	98	5	Y	104	5
6	X	99	5	Y	81	5
7	X	82	5	Y	88	5
8	X	88	5	Y	87	5
9	X	86	5	Y	69	5
10	X	99	6	Y	73	6
11	X	110	6	Y	90	7
12	X	104	6	Y	108	7

Table A.2 Ground Motion Records - SIM24

Station	Direction	PGA (cm/s ²)	Sa (4.07s) (cm/s ²)	Direction	PGA (cm/s ²)	Sa (4.07s) (cm/s ²)
1	X	367	42	Y	258	24
2	X	352	41	Y	216	24
3	X	293	41	Y	311	23
4	X	234	42	Y	282	23
5	X	240	42	Y	235	23
6	X	214	42	Y	219	23
7	X	209	41	Y	238	23
8	X	276	42	Y	204	23
9	X	289	42	Y	178	24
10	X	293	43	Y	209	25
11	X	318	44	Y	228	26
12	X	324	45	Y	223	26

Table A.3 Ground Motion Records - SIM25

Station	Direction	PGA (cm/s ²)	Sa (4.07s) (cm/s ²)	Direction	PGA (cm/s ²)	Sa (4.07s) (cm/s ²)
1	X	207	31	Y	182	27
2	X	174	31	Y	139	24
3	X	142	31	Y	174	24
4	X	156	31	Y	224	24
5	X	168	31	Y	202	25
6	X	138	31	Y	151	26
7	X	137	31	Y	157	26
8	X	148	32	Y	174	25
9	X	139	32	Y	129	25
10	X	161	32	Y	148	26
11	X	202	32	Y	209	27
12	X	207	33	Y	196	28

Table A.4 Ground Motion Records - SIM26

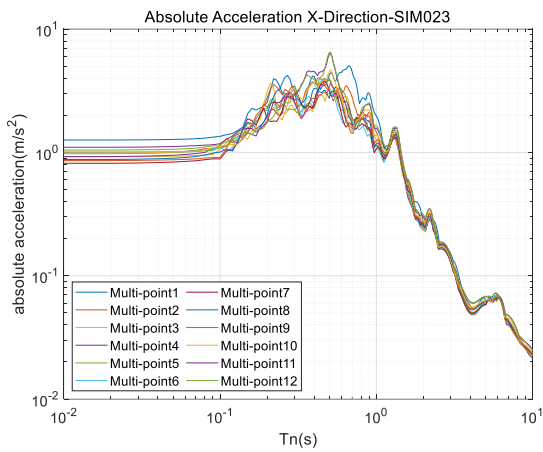
Station	Direction	PGA (cm/s ²)	Sa (3.27s) (cm/s ²)	Direction	PGA (cm/s ²)	Sa (3.27s) (cm/s ²)
1	X	113	12	Y	158	6
2	X	99	12	Y	125	9
3	X	95	12	Y	138	10
4	X	118	11	Y	121	9
5	X	104	12	Y	118	8
6	X	91	11	Y	99	6
7	X	104	11	Y	105	6
8	X	141	11	Y	103	6
9	X	112	11	Y	104	6
10	X	118	11	Y	118	6
11	X	148	11	Y	124	6
12	X	152	11	Y	117	6

Table A.5 Ground Motion Records - SIM27

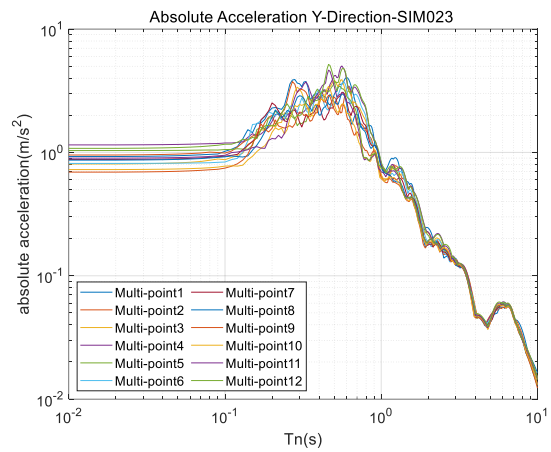
Station	Direction	PGA (cm/s ²)	Sa (4.07s) (cm/s ²)	Direction	PGA (cm/s ²)	Sa (4.07s) (cm/s ²)
1	X	335	39	Y	214	25
2	X	312	37	Y	207	23
3	X	311	35	Y	264	24
4	X	324	34	Y	367	24
5	X	309	33	Y	328	24
6	X	273	32	Y	218	24
7	X	282	32	Y	214	24
8	X	313	32	Y	233	24
9	X	259	32	Y	246	25
10	X	325	32	Y	293	26
11	X	419	32	Y	341	27
12	X	447	33	Y	324	28

Table A.6 Ground Motion Records - SIM28

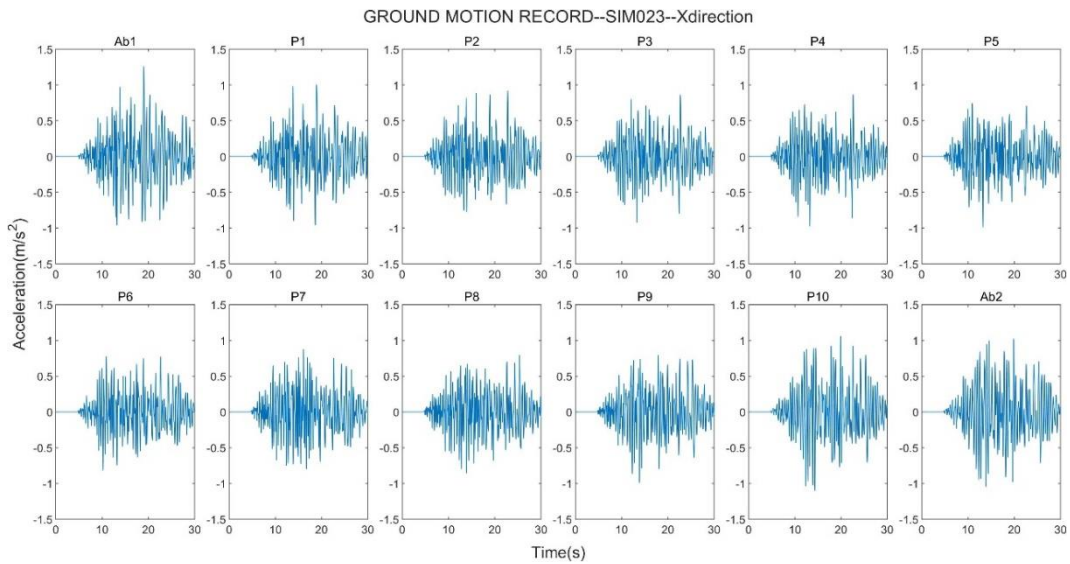
Station	Direction	PGA (cm/s ²)	Sa (4.07s) (cm/s ²)	Direction	PGA (cm/s ²)	Sa (4.07s) (cm/s ²)
1	X	212	29	Y	139	23
2	X	205	28	Y	132	22
3	X	169	28	Y	131	22
4	X	211	28	Y	157	23
5	X	209	28	Y	150	23
6	X	195	28	Y	122	23
7	X	186	28	Y	131	23
8	X	176	29	Y	113	24
9	X	159	29	Y	138	24
10	X	189	30	Y	187	24
11	X	246	30	Y	241	25
12	X	282	30	Y	212	25



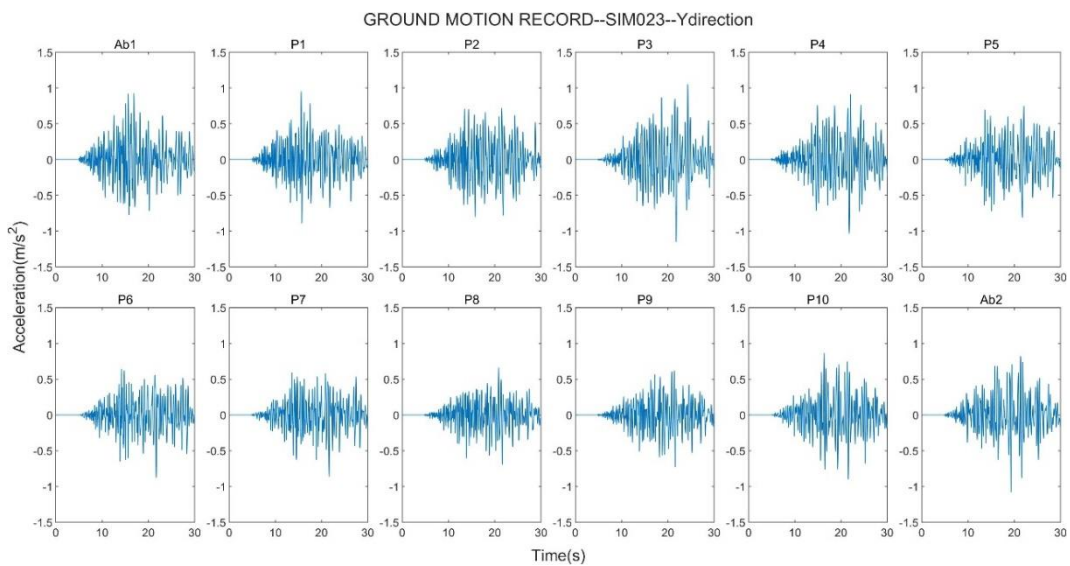
(a) Longitudinal Direction



(b) Transverse Direction

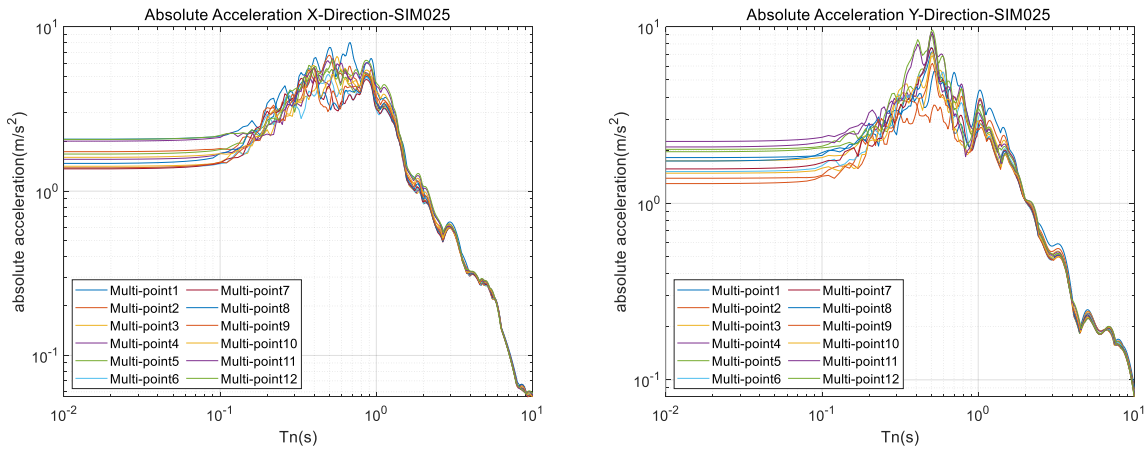


(c) Acceleration Time History of GMs in Longitudinal Direction



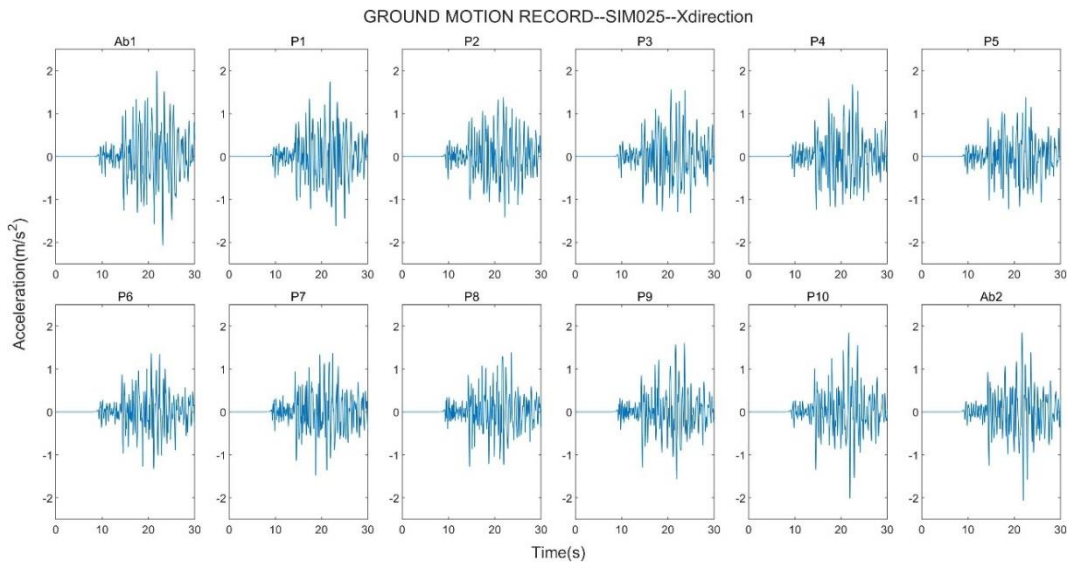
(d) Acceleration Time History of GMs in Transverse Direction

Fig A.1 Response Spectrum and Acceleration Time History for SIM23

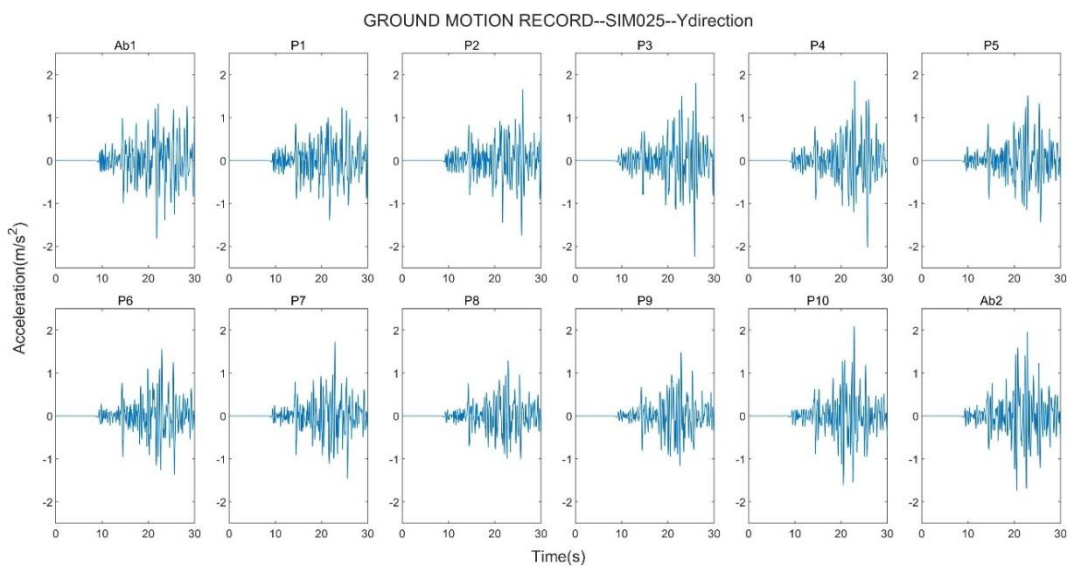


(a) Longitudinal Direction

(b) Transverse Direction

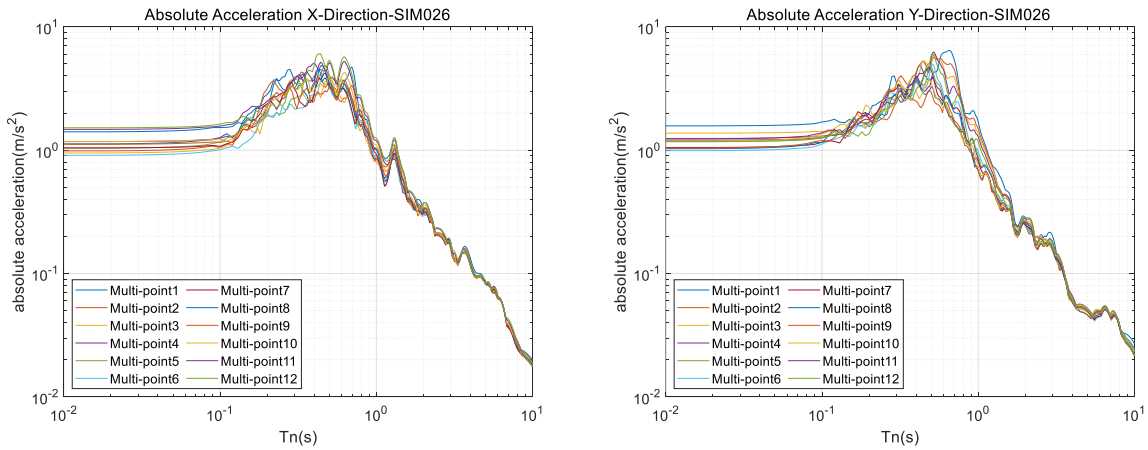


(c) Acceleration Time History of GMs in Longitudinal Direction



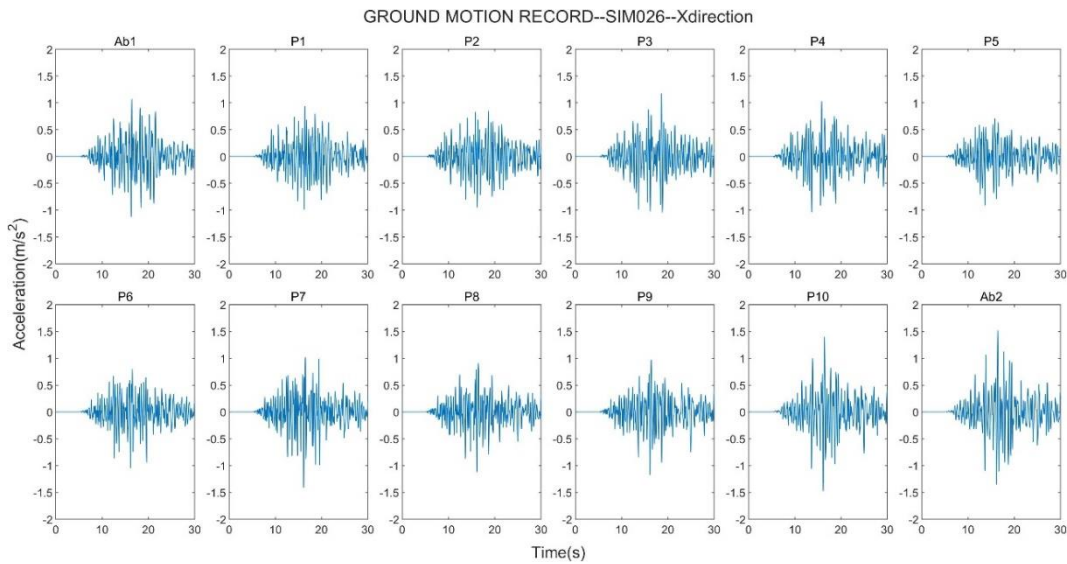
(d) Acceleration Time History of GMs in Transverse Direction

Fig A.2 Response Spectrum and Acceleration Time History for SIM25

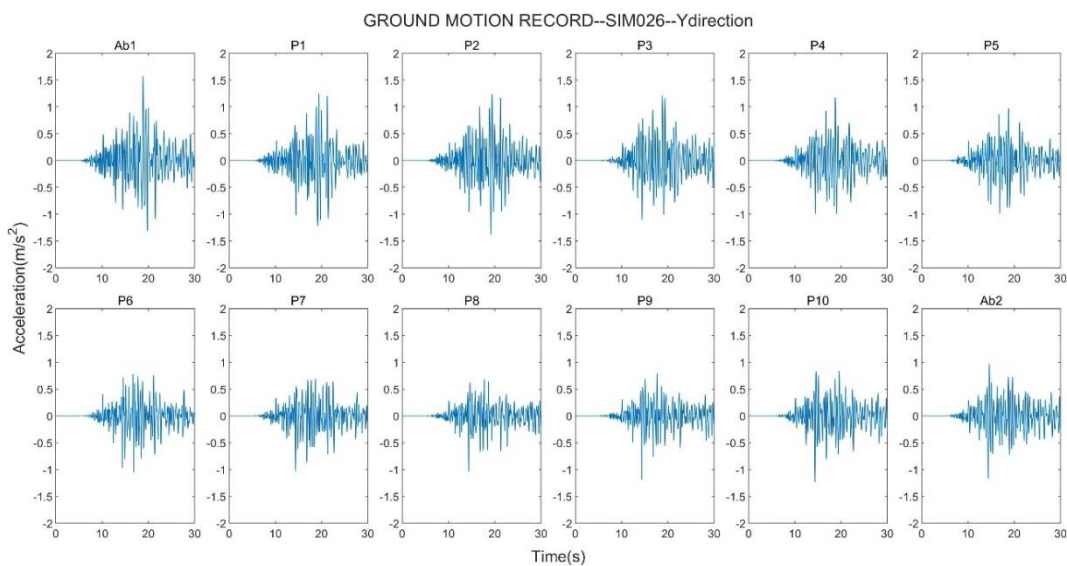


(a) Longitudinal Direction

(b) Transverse Direction

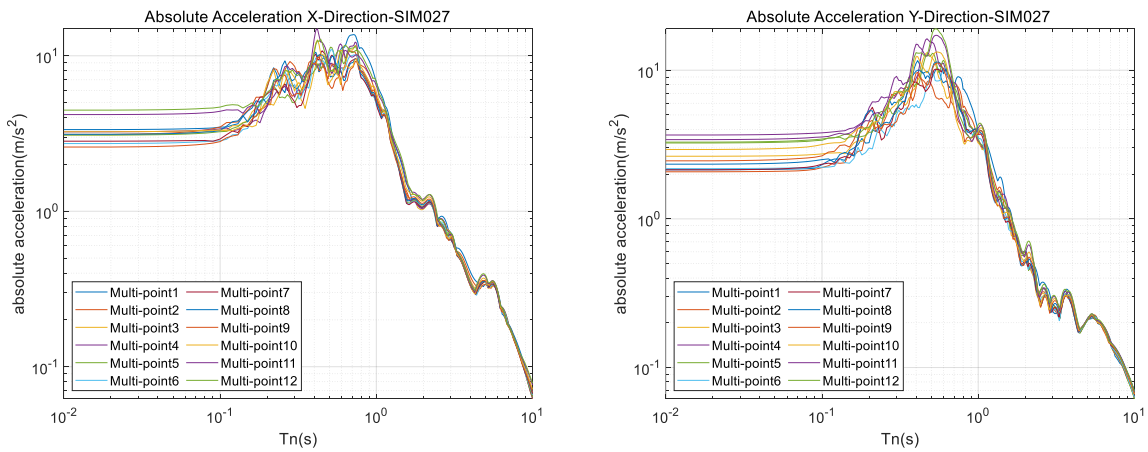


(c) Acceleration Time History of GMs in Longitudinal Direction



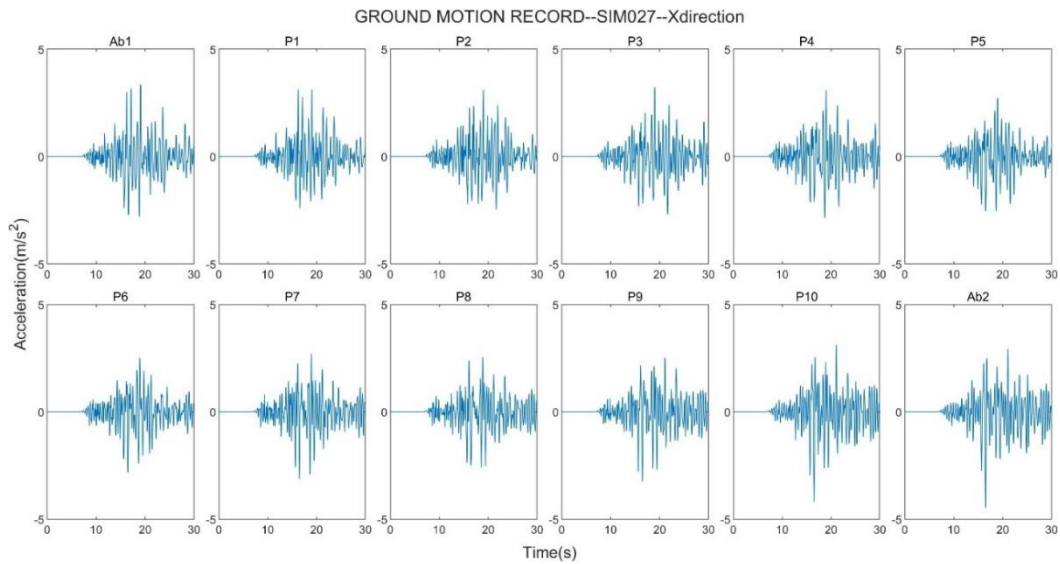
(d) Acceleration Time History of GMs in Transverse Direction

Fig A.3 Response Spectrum and Acceleration Time History for SIM26

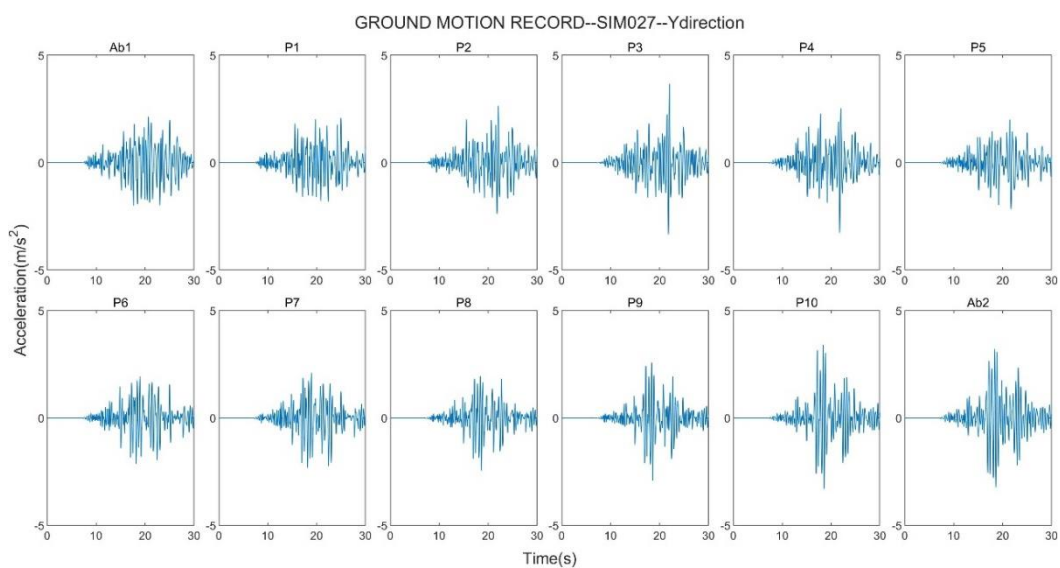


(a) Longitudinal Direction

(b) Transverse Direction

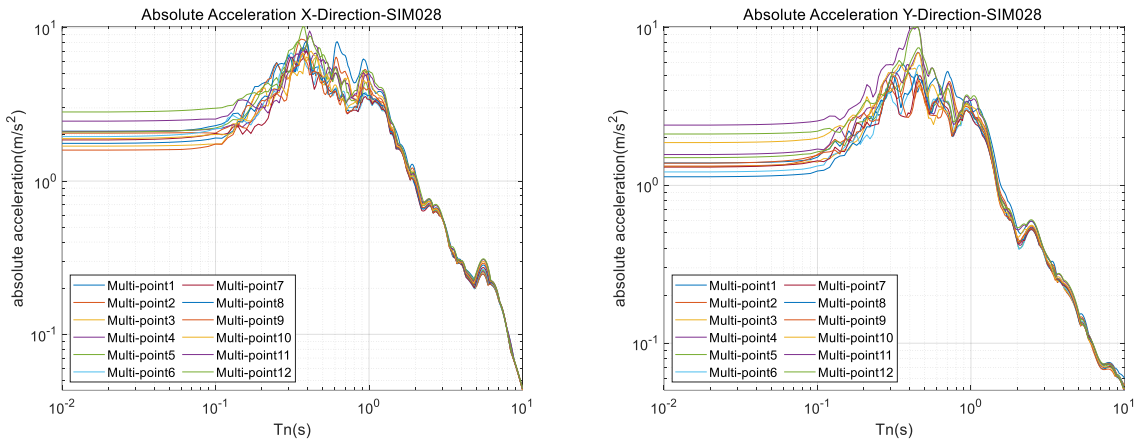


(c) Acceleration Time History of GMs in Longitudinal Direction



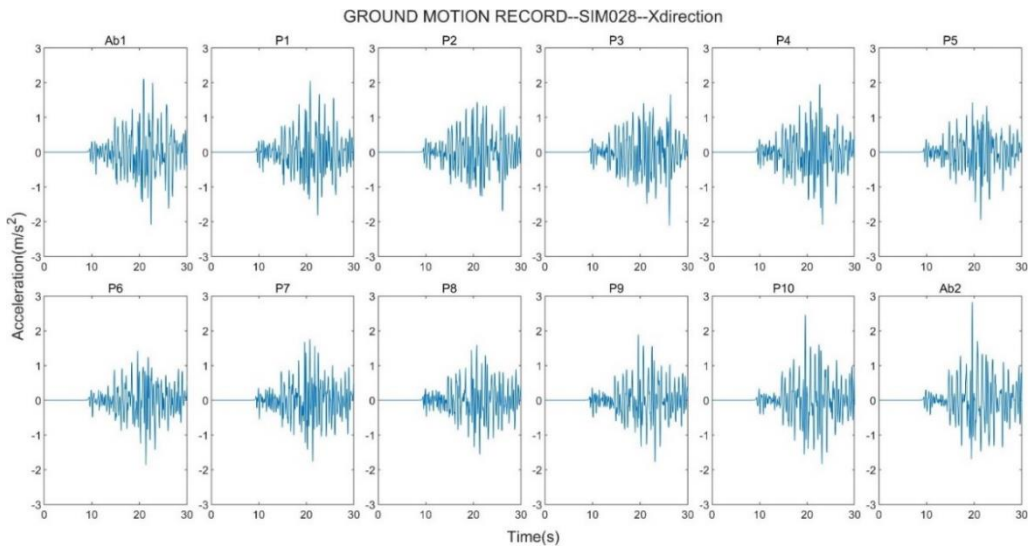
(d) Acceleration Time History of GMs in Transverse Direction

Fig A.4 Response Spectrum and Acceleration Time History for SIM27

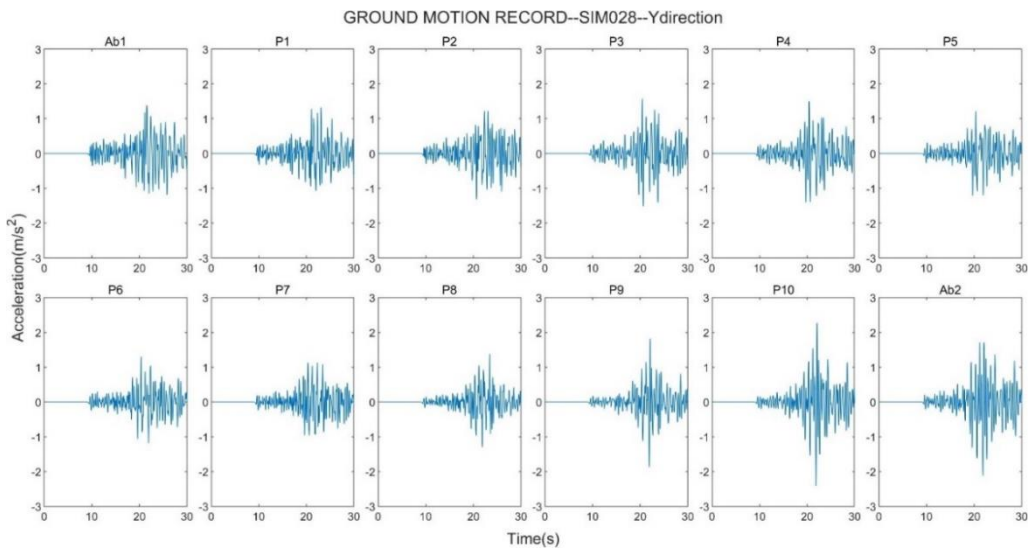


(a) Longitudinal Direction

(b) Transverse Direction



(c) Acceleration Time History of GMs in Longitudinal Direction



(d) Acceleration Time History of GMs in Transverse Direction

Fig A.5 Response Spectrum and Acceleration Time History for SIM28

Appendix B - Responses of Bridge Columns and Bearings

Table B.1 Peak Displacements of Columns under Uniform/Multisupport Excitations - SIM23 (unit: cm)

Column	Case	Displacement		Column	Case	Displacement	
		L	T			L	T
P1	Max	5.6	4.2	P6	Max	0.4	0.3
	Min	4.8	4.2		Min	0.3	0.3
	Multi	4.0	3.5		Multi	0.3	0.3
P2	Max	2.0	0.7	P7	Max	6.7	3.2
	Min	2.0	0.6		Min	3.8	4.1
	Multi	1.0	0.6		Multi	3.8	2.9
P3	Max	0.9	0.4	P8	Max	3.1	2.0
	Min	1.0	0.4		Min	3.6	1.4
	Multi	0.7	0.4		Multi	4.6	1.6
P4	Max	0.5	0.3	P9	Max	5.9	3.3
	Min	0.6	0.3		Min	2.8	2.3
	Multi	0.5	0.2		Multi	2.9	2.4
P5	Max	0.5	0.5	P10	Max	5.3	1.6
	Min	0.4	0.5		Min	2.9	1.4
	Multi	0.4	0.4		Multi	3.7	1.9

**Table. B.2 Peak Displacements of Columns under Uniform/Multisupport Excitations -
SIM25 (unit:cm)**

Column	Case	Displacement		Column	Case	Displacement	
		L	T			L	T
P1	Max	8.8	15.6	P6	Max	0.6	0.7
	Min	7.1	13.8		Min	0.6	0.7
	Multi	8.3	12.3		Multi	0.6	0.7
P2	Max	4.6	2.0	P7	Max	11.5	12.8
	Min	4.0	2.0		Min	9.8	11.8
	Multi	2.8	2.0		Multi	6.6	9.9
P3	Max	3.2	1.7	P8	Max	6.0	5.3
	Min	2.6	1.6		Min	4.2	5.3
	Multi	2.0	1.4		Multi	4.6	4.5
P4	Max	1.7	0.8	P9	Max	8.7	10.0
	Min	1.7	0.7		Min	7.1	7.5
	Multi	1.3	0.7		Multi	8.6	7.2
P5	Max	0.7	0.9	P10	Max	8.1	7.2
	Min	0.8	0.9		Min	6.9	6.4
	Multi	0.7	0.9		Multi	9.8	7.3

**Table. B.3 Peak Displacements of Columns under Uniform/Multisupport Excitations -
SIM26 (unit:cm)**

Column	Case	Displacement		Column	Case	Displacement	
		L	T			L	T
P1	Max	5.5	3.2	P6	Max	0.5	0.3
	Min	3.3	3.8		Min	0.3	0.3
	Multi	4.5	4.7		Multi	0.3	0.2
P2	Max	1.7	0.7	P7	Max	3.8	3.9
	Min	1.2	0.5		Min	2.7	3.9
	Multi	1.0	0.5		Multi	2.6	3.2
P3	Max	0.7	0.3	P8	Max	4.6	1.7
	Min	0.7	0.3		Min	3.1	1.9
	Multi	0.7	0.3		Multi	3.6	1.5
P4	Max	0.6	0.3	P9	Max	4.6	2.2
	Min	0.5	0.3		Min	3.3	2.8
	Multi	0.6	0.2		Multi	4.3	1.8
P5	Max	0.6	0.5	P10	Max	4.0	2.0
	Min	0.4	0.4		Min	3.2	1.9
	Multi	0.3	0.3		Multi	4.4	2.2

**Table. B.4 Peak Displacements of Columns under Uniform/Multisupport Excitations -
SIM27 (unit:cm)**

Column	Case	Displacement		Column	Case	Displacement	
		L	T			L	T
P1	Max	13.6	15.0	P6	Max	1.3	0.8
	Min	10.5	9.8		Min	0.9	0.7
	Multi	15.9	11.1		Multi	0.8	0.7
P2	Max	3.8	2.6	P7	Max	18.3	16.4
	Min	3.5	2.0		Min	13.1	11.3
	Multi	4.0	2.0		Multi	9.7	11.2
P3	Max	3.0	1.7	P8	Max	7.0	4.8
	Min	2.1	1.4		Min	9.2	4.1
	Multi	2.8	1.6		Multi	7.0	4.7
P4	Max	2.3	0.7	P9	Max	19.0	9.2
	Min	1.5	0.7		Min	20.2	7.0
	Multi	1.8	0.7		Multi	21.0	9.2
P5	Max	1.8	0.9	P10	Max	15.9	8.7
	Min	1.2	0.9		Min	19.7	6.9
	Multi	1.2	0.9		Multi	19.5	7.6

**Table. B.5 Peak Displacements of Columns under Uniform/Multisupport Excitations-
-SIM28 (unit: cm)**

Column	Case	Displacement		Column	Case	Displacement	
		L	T			L	T
P1	Max	11.2	13.0	P6	Max	0.8	0.7
	Min	6.8	12.4		Min	0.8	0.7
	Multi	8.3	10.8		Multi	0.8	0.7
P2	Max	3.7	2.3	P7	Max	13.0	11.1
	Min	3.6	2.1		Min	10.6	10.9
	Multi	3.2	1.8		Multi	7.5	10.9
P3	Max	2.6	1.4	P8	Max	5.8	4.7
	Min	2.8	1.3		Min	5.5	5.1
	Multi	2.7	1.2		Multi	4.1	4.9
P4	Max	1.9	0.9	P9	Max	5.5	8.2
	Min	2.1	0.9		Min	5.6	6.5
	Multi	2.0	0.8		Multi	6.5	6.1
P5	Max	1.1	1.0	P10	Max	5.2	8.2
	Min	1.0	0.9		Min	5.3	5.8
	Multi	1.1	0.9		Multi	8.1	7.4

**Table. B.6 Peak Displacements of Bearings under Uniform/Multisupport Excitations
– SIM23 (unit: cm)**

Bearing	Case	Displacement		Bearing	Case	Displacement	
		L	T			L	T
P1	Max	5.5	2.0	P6	Max	3.1	5.6
	Min	4.8	3.2		Min	2.3	5.7
	Multi	4.7	1.4		Multi	2.6	4.1
P2	Max	1.6	3.3	P7	Max	5.8	3.8
	Min	1.6	3.2		Min	3.6	3.7
	Multi	1.4	3.2		Multi	3.3	2.7
P3	Max	2.5	3.6	P8	Max	7.5	3.2
	Min	1.8	3.9		Min	7.1	2.5
	Multi	1.5	3.6		Multi	8.2	2.4
P4	Max	2.7	5.0	P9	Max	7.1	2.6
	Min	1.8	4.9		Min	4.0	1.8
	Multi	1.7	3.8		Multi	4.2	2.6
P5	Max	3.0	5.9	P10	Max	7.6	1.5
	Min	2.1	5.9		Min	4.2	1.1
	Multi	2.3	3.9		Multi	4.9	1.9

**Table.B.7 Peak Displacements of Bearings under Uniform/Multisupport Excitations -
SIM25 (unit: cm)**

Bearing	Case	Displacement		Bearing	Case	Displacement	
		L	T			L	T
P1	Max	10.2	4.4	P6	Max	8.5	21.6
	Min	7.8	3.1		Min	7.9	20.8
	Multi	9.5	3.0		Multi	8.5	18.0
P2	Max	4.0	14.7	P7	Max	12.3	8.0
	Min	3.7	13.6		Min	10.4	7.8
	Multi	3.5	11.4		Multi	8.5	8.3
P3	Max	5.5	15.6	P8	Max	11.6	8.3
	Min	5.0	14.2		Min	10.6	8.2
	Multi	4.5	14.7		Multi	13.1	7.2
P4	Max	6.2	11.7	P9	Max	13.3	8.5
	Min	5.9	10.9		Min	10.5	5.1
	Multi	5.7	11.4		Multi	11.9	6.3
P5	Max	7.6	18.0	P10	Max	12.9	6.3
	Min	7.4	17.5		Min	10.4	4.7
	Multi	7.4	15.5		Multi	13.8	6.4

**Table. B.8 Peak Displacements of Bearings under Uniform/Multisupport Excitations -
SIM26 (unit: cm)**

Bearing	Case	Displacement		Bearing	Case	Displacement	
		L	T			L	T
P1	Max	5.9	2.2	P6	Max	2.5	5.4
	Min	3.5	1.8		Min	1.8	5.0
	Multi	4.3	3.0		Multi	2.0	3.5
P2	Max	1.7	3.3	P7	Max	3.2	3.4
	Min	1.2	2.7		Min	2.4	4.7
	Multi	1.3	2.9		Multi	2.8	3.4
P3	Max	1.8	2.9	P8	Max	8.4	2.8
	Min	1.4	2.6		Min	5.9	3.1
	Multi	1.4	2.9		Multi	6.3	2.4
P4	Max	2.1	4.8	P9	Max	6.9	2.7
	Min	1.5	3.8		Min	4.9	2.2
	Multi	1.5	3.5		Multi	5.7	2.3
P5	Max	2.5	5.6	P10	Max	6.0	2.1
	Min	1.8	4.8		Min	4.6	2.0
	Multi	1.9	3.4		Multi	5.8	2.3

**Table. B.9 Peak Displacements of Bearings under Uniform/Multisupport Excitations -
SIM27 (unit: cm)**

Bearing	Case	Displacement		Bearing	Case	Displacement	
		L	T			L	T
P1	Max	14.7	13.5	P6	Max	12.4	14.5
	Min	11.4	6.5		Min	8.6	14.0
	Multi	16.1	6.5		Multi	10.4	13.1
P2	Max	6.2	12.3	P7	Max	14.2	19.0
	Min	4.2	8.9		Min	9.9	10.9
	Multi	5.2	9.0		Multi	8.6	11.3
P3	Max	6.4	15.5	P8	Max	15.3	7.5
	Min	4.3	12.1		Min	20.1	6.0
	Multi	5.5	13.0		Multi	15.8	6.4
P4	Max	8.2	13.4	P9	Max	26.4	7.9
	Min	5.4	12.5		Min	27.0	6.2
	Multi	7.0	12.6		Multi	30.6	7.9
P5	Max	11.5	13.7	P10	Max	22.9	7.5
	Min	7.8	13.1		Min	25.1	4.9
	Multi	9.3	11.3		Multi	28.2	5.8

**Table. B.10 Peak Displacements of Bearings under Uniform/Multisupport Excitations
- SIM28 (unit: cm)**

Bearing	Case	Displacement		Bearing	Case	Displacement	
		L	T			L	T
P1	Max	11.7	5.0	P6	Max	10.1	17.7
	Min	6.7	4.0		Min	8.0	18.9
	Multi	7.2	2.2		Multi	7.4	17.4
P2	Max	4.7	13.8	P7	Max	13.1	8.0
	Min	4.1	11.8		Min	10.6	7.5
	Multi	3.8	10.0		Multi	9.2	7.5
P3	Max	6.6	16.1	P8	Max	14.6	7.7
	Min	5.3	13.2		Min	10.2	7.3
	Multi	4.4	12.4		Multi	11.1	7.3
P4	Max	7.7	13.7	P9	Max	9.9	6.7
	Min	5.8	13.1		Min	9.7	4.7
	Multi	5.2	11.3		Multi	9.0	4.8
P5	Max	9.5	15.3	P10	Max	10.3	7.0
	Min	7.6	16.8		Min	9.5	4.6
	Multi	7.0	14.9		Multi	11.1	6.5